Hepatic inflammation elicits production of proinflammatory netrin-1 through exclusive activation of translation

Romain Barnault, Claire Verzeroli, Carole Fournier, Maud Michelet, Anna Rita Redavid, Ievgeniia Chicherova, Marie-laure Plissonnier, Annie Adrait, Olga Khomich, Fleur Chapus, et al.

Hepatic inflammation elicits production of proinflammatory netrin-1 through exclusive activation of translation

Romain Barnault[1#], Claire Verzeroli[1#], Carole Fournier[2], Maud Michelet[1], Anna Rita Redavid[3], Ievgeniia Chicherova[1], Annie Adrait[4], Olga Khomich[1], Fleur Chapus[1], Mathieu Richaud[1], Federica Grazia Centonze[5], Julie Lucifora[1], Birke Bartosch[1], Michel Rivoire[6], Hesso Farhan[5], Yohann Couté[4], Valbona Mirakaj[7], Thomas Decaens[2], Patrick Mehlen[3], Benjamin Gibert[3], Fabien Zoulim[1,8], Romain Parent[1*]

[1] Pathogenesis of Chronic Hepatitis B and C laboratory - LabEx DEVweCAN, Inserm U1052, Cancer Research Centre of Lyon, F-69003 Lyon, France, University of Lyon, F-69003 Lyon, University of Lyon 1, ISPB, Lyon, F-69622, France, CNRS UMR5286, F-69083 Lyon, France, Centre Léon Bérard, F-69008 Lyon, France

[2] Institute for Advanced Biosciences, Inserm U1209, University of Grenoble-Alpes, F-38700 La Tronche, France

[3] Apoptosis, Cancer and Development Laboratory - LabEx DEVweCAN, Inserm U1052, Cancer Research Centre of Lyon, F-69003 Lyon, France, University of Lyon, F-69003 Lyon, University of Lyon 1, ISPB, Lyon, F-69622, France, CNRS UMR5286, F-69083 Lyon, France, Centre Léon Bérard, F-69008 Lyon, France

[4] University of Grenoble-Alpes, Inserm, CEA, UMR BioSanté U1292, CNRS CEA FR2048, F-38000, Grenoble, France

[5] Institute of Basic Medical Science, University of Oslo, N-0372, Oslo, Norway

[6] Léon Bérard Cancer Center, F-69008 Lyon, France, Université Lyon 1, Lyon, F-69622, France

[7] Department of Anesthesiology and Intensive Care Medicine, University Hospital Tübingen, Eberhard-Karls-University, DE-72076, Tuebingen, Germany.

[8] Hospices Civils de Lyon, Service of hepato-gastroenterology, F-69001 Lyon, France

[#] Equal contributions

* Corresponding author

Abstract

Causal links between inflammation and cancer are well-established, and research into the means of controlling the former is paramount. Netrin-1 is targeted in clinical trials as it displays pro-tumoral properties in inflammatory contexts in some organs, which led us to investigate its status with respect to inflammation in the liver. Here, based on a positive clinical correlation between netrin-1 levels and inflammation, experimentally confirmed in mice by inducing inflammation using poly(I:C) as a TLR3 agonist, we identify netrin-1 as a hepatic inflammation-inducible factor and decipher its underlying mechanism. Surprisingly, netrin-1 upregulation relied on a hitherto unknown mode of induction, namely its exclusive translational activation following the transfer of *NTN1* to the ER, ruling out any other traditional processes through exhaustive approaches. Our *in vitro* approaches unveiled a direct interaction between the Staufen-1 protein and netrin-1 mRNA, and were further validated in mice. Based on these findings, we finally explored the impact of a phase 2 clinical trial-validated humanized anti-netrin-1 antibody (NP137) on mice livers, and observed a clear anti-inflammatory activity. Hence, our results provide a better understanding of the interplay between inflammation and chronic liver disease and offer an innovative therapeutic perspective for interfering with their adverse evolution.

Introduction

Chronic liver diseases (CLDs) represent the main etiological conditions for the onset of liver injury, cirrhosis, and hepatocellular carcinoma (HCC) [1]. Though CLDs exhibit a high degree of diversity in terms of causal effects, ranging from infectious (hepatitis B and C viruses, HBV and HCV), to metabolic, to toxic and finally genetic, they all converge towards hepatic inflammation. This response in turn drives hepatocytic turnover, extracellular matrix accumulation, histological worsening and the long-term induction of carcinogenic mediators eventually leading to the development of HCC [2]. A clear understanding of the outcome of this inflammatory response and of its onset in the hepatic tissue is hampered by biologically opposite functions, as it favors viral and dead cell clearance, as well as histological wound healing, but exacerbates fibrogenesis, thus inducing cirrhosis and oncogenesis. Hence, the identification of factors involved in a harmful regulation of inflammation may lead to its clinical improvement.

We previously documented the pathogenic implication of netrin-1, a developmentally-regulated and secreted factor of neural origin [3], in liver diseases. Indeed, we showed that the expression of this factor is reactivated in several illnesses in adulthood, including several types of carcinomas [4-7] and also induced by HBV and HCV [8, 9]. Netrin-1 is well-known for preventing cellular apoptosis through its binding to 'dependence receptors' [5, 6, 10-15], and we demonstrated that it endowed hepatocytes with resistance to apoptosis during the unfolded protein response (UPR) [16], a hallmark of CLDs and cirrhosis [17-19]. Owing to the causal link between inflammation, cancer in general, and HCC, we hypothesized that hepatic inflammation and netrin-1 may be reciprocal influencers in the liver.

Owing to conflicting data on the implication of netrin-1 in inflammation, by either exacerbating [20-22] or dampening [23-25] the inflammatory response according to the chronic inflammation setting studied, we conducted extensive mechanistic experiments to document its implication in this organ, similarly to that described in inflammatory bowel disease and colorectal cancer [6, 26]. We first confirmed a clinical correlation between inflammation and netrin-1 upregulation in a cohort of HBV samples, which we then validated in mice using poly(I:C) to induce inflammation. Through a series of experiments on HepaRG cells and PHH, including polysomal isolation and fractionation, SILAC metabolic incorporation, and direct interaction assays, we dissected each step of netrin-1 biogenesis to comprehend its induction. We unveiled the implication of the Staufen-1 protein in netrin-1 mRNA localization at the ER, fostering its translation activation and identified distinct yet converging mechanisms in both hepatocytic environments. Finally, we confirmed these data in mice through netrin-1 capture experiments using a phase I and II clinical trial-validated (NCT02977195) humanized antibody [27] that reversed hepatic inflammation *in vivo*. Hence, we show that netrin-1 is a newly identified

hepatic inflammation-inducible factor endowed with pro-inflammatory properties, and that an antibody enabling netrin-1 capture may dampen hepatic inflammation, a dataset of general interest in CLD.

Material and methods

Clinical samples

Clinical liver samples were used under the French IRB 'CPP South-East IV' approval #A16/207 (2016) related to the Inserm unit 1052 Hepatology biobank, France (#DC2008-235). Written informed consent was obtained from each patient and conformed to the ethics guidelines of the 1975 Declaration of Helsinki. Sample characteristics are shown in the **Suppl. Table 1.** All activity scores were determined by the pathology department of the Lyon University Hospital using standardized procedures.

Animal housing, treatment and sample harvest

All trials were performed under IRB agreement #CECCAP_CLB_2014_015 as previously described (doi 10.15252/emmm.202012878). Eight-week-old C57BL/6J mice (Janvier Laboratories, Saint Berthevin, France) were injected intraperitoneally with poly(I:C) (Invivogen, Toulouse, France) at indicated doses or PBS for 16 h and sacrificed prior to liver harvest. Due to liver zonation considerations [28], all analyses were performed after selection on ice of the median hepatic lobe of all animals. Hepatic lobe samples were immediately snap frozen in liquid nitrogen and subsequently thawed on ice prior to homogenization using a Dounce apparatus previously refrigerated, followed by the addition of RIPA or polysome buffer (see below, protein or polysome-related studies) or Trizol (see below, total RNA-related studies, Invitrogen).

Immunohistochemistry

For histological examination, tissue samples were fixed in 10% buffered formalin and embedded in paraffin, and prepared according to conventional procedures. Immunohistochemistry was performed on an automated immunostainer (Ventana Discovery XT, Roche, Meylan, France) using the Discovery HRP Kit according to the manufacturer's instructions. Sections were incubated with an anti-netrin-1 antibody (1/500; see **Suppl. Table 2**). Staining was visualized with DAB solution with 3,3′-diaminobenzidine as a chromogenic substrate. Finally, the sections were counterstained with Gill's hematoxylin.

Flow cytometry analysis

Pieces of liver were minced and digested in RPMI-1640 supplemented with mouse tumor dissociation enzymes (Miltenyi Biotec, Bergisch Gladbach, Germany) for 40 min at 37°C. Digested samples were filtered through a 70 µm nylon mesh to obtain uniform single-cell suspensions. Cells were washed with complete RPMI medium containing 10% decomplemented FBS, 1% NEAA, 1% Sodium Pyruvate and 1% Penicillin-Streptomycin

(Gibco™) and resuspended in 500 µL of Flow Cytometry Staining Buffer (FCSB) (eBioscience™). 100 µL of cell suspension was used for staining in U-shaped 96-well plates. After PBS 1X washing, cells were stained with LIVE/DEAD™ Fixable Red Dead Cell Stain Kit for 30 min protected from light at room temperature. Fc receptors were blocked with anti-CD16/CD32 (TruStain FcX™; Biolegend) and cells were stained for cell surface antigens (see **Suppl. Table 2**). For intracellular staining, cells were fixed and permeabilized using the Foxp3 / Transcription Factor Staining Buffer Set (eBioscience™). Events were acquired on a BD-LSRII flow cytometer (BD Biosciences, Le Pont-De-Claix, France), collected with the BD FACSDiva 6.3.1 software and analyzed using Flowjo (or Flowlogic) software.

Cell culture and siRNA/plasmids transfection

Cells were grown in a 5% CO_2 humidified atmosphere at 37°C. All reagents pertaining to HepaRG cell culture were purchased from ThermoFischer Scientific (Les Ulis, France) unless otherwise indicated. HepaRG cells were seeded at a density of $4.10^4/cm^2$ in William's E medium containing insulin 5 mg/mL, penicillin 100 IU/mL, streptomycin 100 mg/mL, and 10% fetal bovine serum (Hyclone, Illkirch, France). The medium was supplemented with hydrocortisone hemisuccinate at a concentration of 5.10^{-5} mol/L (Pharmacia Upjohn, Guyancourt, France). Medium was renewed twice a week. siRNAs (Flexitube, Qiagen, Les Ulis, France, **Suppl. Table 3**) and plasmids were transfected using RNAiMax (Thermo, Les Ulis, France) or Mirus LT1 reagents (Mirus-Bio, Euromedex, Souffelweyersheim, France), following the manufacturer's procedures at a final concentration of 10 nM and 1 µg/mL, respectively. All transfections were performed in suspension before distribution in wells and poly(I:C) treatment in order to prevent transfection yield variability. Primary human hepatocytes (PHHs) were isolated from surgical liver resections, after informed consent of patients (IRB agreements #DC-2008-99 and DC-2008-101) as previously described [29] and cultured in complete William's medium supplemented with 1.8% DMSO (Sigma, St Quentin, France). All PHH-related data were obtained from at least three distinct patients. For TLR3-specific or pan-TLR stimulation, cells were treated with Pam3-CSk4, LPS, FLA, FSL, Riboxol and LMW or HMW poly(I:C) (InvivoGen, Toulouse, France) three to four days after seeding (*i.e.* after having reached confluency) for the indicated time points and/or concentrations.

Cell viability assays

The Neutral Red (NR) assay was conducted as described by Repetto [30]. Briefly, the NR stock solution (40 mg NR dye in 10 mL PBS) was diluted in culture medium to a final concentration of 4 mg/mL and then centrifuged at 600*g* for 10 min to remove any precipitated dye crystals. Cells were then incubated with 100 µL of NR medium for 1 h. NR medium was removed and the cells washed with PBS. Plates were incubated for 10 min under shaking with

150 µL/well of NR destain solution (50% ethanol 96%, 49% deionized water, 1% glacial acetic acid). OD at 540 nm was measured.

Western blotting

Immunoblotting was performed using 40 µg of RIPA (50 mM Tris HCl (pH 8.0), 150 mM NaCl, 1% NP-40, 0.5% sodium deoxycholate, 0.1% SDS, 10 mM sodium fluoride, 50 mM orthovanadate, 1x protease inhibitor cocktail (Roche))-processed cell lysates, then resolved on 8% or 10% SDS-PAGE, blotted onto nitrocellulose membranes (Amersham Biosciences), blocked using 5% low fat dried milk in TBS Tween 0.1% for 1 hour at RT and probed overnight at 4°C with corresponding antibodies listed in the **Suppl. Table 2**. After three washes in PBS-Tween 0.1%, membranes were incubated for 1 h at room temperature with secondary antibodies coupled to HRP (1/5,000, Sigma-Aldrich, St-Quentin, France) prior to chemiluminescence-based revelation using the Clarity Western ECL substrate (Bio-Rad, Versailles, France). The Western blot specificity of the netrin-1 antibody was extensively verified in-house prior to conducting experiments (**Suppl. Fig. 1**).

Immunofluorescence

Cells were fixed in -20°C methanol/acetone after one wash of ice-cold PBS, blocked in 5% goat serum (Eurobio, Les Ulis, France) at room temperature for 15 min, incubated overnight with corresponding antibodies listed in **Suppl. Table 2** in PBS/0.1% Triton X-100, washed prior to incubation with secondary antibodies listed in the **Suppl. Table 2**, mounted with DAPI. Cells were finally visualized under a confocal microscpoe (Leica SP5X, magnification 63X, Zoom = 2).

Netrin-1 immunoprecipitation

For netrin-1 immunoprecipitation from tissue culture medium, serum-free medium complemented or not with heparin (2 µg/mL, Sigma-Aldrich, France), was applied to the cells overnight, 60 h after poly(I:C) treatment. 5x or 1x lysis buffer (20 mM Tris pH 7.5, 150 mM NaCl, 1 mM EDTA, 1 mM EGTA, 0.1% Triton X-100, Protease inhibitor cocktail 1x) were used for supernatant or total lysates immunoprecipitation, respectively. Two µg of anti-netrin-1 NP137 antibody [27] / 5 mL of medium or 2 µg NP137 / mg of protein extracted from total lysates were incubated overnight on a rotating wheel at 4°C. Twenty µL of SureBeads™ Protein A Magnetic Beads (Biorad) was added for 2µg of antibody, for 1 h on a rotating wheel at 4°C. Beads were then washed three times with lysis buffer 1x and eluted in 20 µL of 1x Laemmli buffer for 5 min at 95°C (Staufen-1, Netrin-1 IP) or extracted with acid phenol (Invitrogen) reagent followed by proteinase K extraction (Staufen-1 IP) as described earlier [31].

Total RNA extraction and RT-qPCR

Total RNA was extracted using Trizol (Invitrogen). One µg of RNA was DNAse I-digested (Promega, Charbonnières, France) and then reverse transcribed using MMLV reverse transcriptase (ThermoFischer) according to the manufacturer's instructions. Pre-mRNA-targeting qPCR was tested for absence of DNA-based qPCR signal upon heat inactivation of MMLV. Quantitative real-time PCR was performed on 1/5th diluted samples on a LightCycler 96 device (Roche, Meylan, France) using the low Rox qPCR mix (Bioline, Paris, France). PCR primer sequences (5′-3′) and qPCR conditions are listed in the *ad hoc* section. Specificity of all primers (**Suppl. Table 4**) was assessed by melting curve analyses and agarose gel electrophoresis. Performance of all primers was quantified using serial 3-fold dilutions of target templates.

Nascent RNA capture

Cells were treated with 0.2 mM ethynyl uridine (EU) for 24 h in order to obtain nascent RNAs with an incorporated EU label. Total RNAs were isolated with Tizzol (Invitrogen). The EU-labeled RNAs were biotinylated and captured using the Click-it Nascent RNA Capture Kit (Life Technologies), in accordance with the manufacturer's instructions. One µg of total RNA was used for biotinylation with 0.25 mM biotin azide in the Click-iT reaction buffer. The RNAs were precipitated with ammonium acetate and ethanol and resuspended in UltraPure water. EU-labeled biotinylated RNAs were captured using Dynabeads MyOne Streptavidin T1 magnetic beads. 0.5 µg of biotinylated RNAs was mixed with Click-iT RNA binding buffer and heated at 68°C for 5 min, followed by the addition of the beads (25 µL of suspension per reaction) and incubation at room temperature for 30 min while gently vortexing. The beads were immobilized using the DynaMag-2 magnet and were washed with Click-iT washing buffers 1 and 2. The washed beads were resuspended in Click-iT wash buffer 2 and used for cDNA synthesis.

Sequential extraction

This protocol followed Stephens et al. [32, 33] using the following buffer compsitions. Permeabilization: 110mM KOAc, 25mM KHEPES pH7.2, 2.5mM Mg(OAc)2, 1 mM EGTA, 0.015% digitonin, 1 mM DTT, 1 mM PMSF, 200µM VRC. Wash: 110 mM KOAc, 25 mM KHEPES pH 7.2, 2.5 mM Mg(OAc)2, 1 mM EGTA, 0.004% digitonin, 1 mM DTT, 1 mM PMSF, 200µM VRC. Lysis: 400 mM KOAc, 25 mM KHEPES pH 7.2, 15 mM Mg(OAc)2, 1% (v/v) NP-40, 0.5% (w/v) DOC, 1 mM DTT, 1 mM PMSF, 200µM VRC. Briefly, aspiration of medium and washing of cells (100 mm Petri dishes) with 5-10 mL ice-cold PBS to remove any excess culture medium was first conducted. Flasks were then gently coated with digitonin-containing 1 mL permeabilization buffer and shaken at 4°C on ice for 5 min. At this point, loss of plasma

membrane and soluble cytosolic contents could be observed using phase contrast microscopy (**Suppl. Fig. 2A**). The flasks were then straightened (vertical position) and the buffer allowed to drain for 1 min. The soluble material (cytosol) was transferred to a 1.5 mL microcentrifuge tube on ice, before gently washing the flasks with 5 mL of digitonin-free wash buffer, which was then discarded. The flasks were next coated with 1 mL of NP40-containing lysis buffer and shaken on ice for 5 min. At this point, only nuclei and insoluble cytoskeletal components remain attached to the culture flask, which once again could be visualized using routine phase contrast microscopy (**Suppl. Fig. 2B**). The flasks were subsequently straightened and the buffer allowed to drain for 1 min. The resulting soluble (membrane-bound) material was transferred to a 1.5 mL microcentrifuge tube. Finally, soluble lysates were clarified at 10,000*g* for 10 min at 4°C and the supernatants transferred to new tubes.

Polysome isolation and profiling

For polysome fractionation, cycloheximide (Sigma, 100µg/ml; Interchim, Montluçon, France) was added to the medium for 5 and/or 15 min, prior to harvesting. The medium was then removed and the cells washed with ice-cold PBS containing 100 µg/mL cycloheximide. The cells were then scraped, centrifuged at 800*g* for 5 min at 4°C and cytoplasmic RNA was obtained by lysis (20 strokes of a p1000 pipet) of the cell pellet in 1 mL of polysome buffer containing 10 mM Tris-HCl (pH 8.0), 140 mM NaCl, 1.5 mM MgCl2, 0.5% Nonidet P-40, and 40 mM vanadyl ribonucleoside complexes (VRC), 100 µg/mL cycloheximide (CHX), 20 mM dithiothreitol (DTT), and 1 mM phenylmethanesulfonyl fluoride (PMSF), all reagents were supplied by Sigma. Mitochondria and membrane debris were removed by centrifugation (10,000*g*, 5 min, 4°C). The post-mitochondrial supernatants were overlaid onto a 15-40% sucrose gradient and spun at 38,000rpm for 2 h at 4°C in a SW41Ti rotor (Beckman Coulter, Fullerton, CA, USA). Fractions were collected from the top of each gradient using a 240 nm UV reader-coupled fraction collector (Brandel, Glasgow, UK). Free mRNPs, monosomes and polysomes were located through the interpretation of UV gradient traces. RNA extraction was done using the acid phenol approach detailed previously [8].

Mass spectrometry-based proteomic analyses

The gel bands containing immunocaptured netrin-1 from the three independent experiments were cut and digested in-gel using trypsin (modified, sequencing purity, Promega), as previously described [34]. The resulting peptides were analyzed by online nanoliquid chromatography coupled to MS/MS (Ultimate 3000 RSLCnano and Q-Exactive HF, Thermo Fisher Scientific) using a 60 min gradient. For this purpose, the peptides were sampled on a pre-column (300 µm x 5 mm PepMap C18, Thermo Scientific) and separated in a 75 µm x 250

mm C18 column (Reprosil-Pur 120 C18-AQ, 1.9 µm, Dr. Maisch). The MS and MS/MS data were acquired by Xcalibur (Thermo Fisher Scientific).

Peptides and proteins were identified and quantified using MaxQuant (version 1.6.17.0) [35] using the Uniprot database (*Homo sapiens* taxonomy, May 2020 version) and the frequently observed contaminant database embedded in MaxQuant. Trypsin was chosen as the enzyme and two missed cleavages were allowed. Peptide modifications allowed during the search were: carbamidomethylation (C, fixed), acetylation (Protein N-ter, variable) and oxidation (M, variable). Minimum peptide length and minimum number of unique peptides were set at seven amino acids and one, respectively. Maximum false discovery rates - calculated by employing a reverse database strategy - were set at 0.01 of the peptide-spectrum match, peptide and protein levels. The netrin-1 ratio in heavy over medium forms (replicates 1 and 3) or medium over heavy forms (replicate 2) were calculated for each replicate based on the corresponding peptide ratios.

CLIP assay

Poly(I:C) treated and mock cells were supplemented with 100 µg/mL cycloheximide (5 min. 37°C), then washed with ice-cold PBS, fixed under UV light (0.2 J/cm^2), scraped with ice-cold PBS, spun down at 1,000*g* for 5 min at 4°C and snap-frozen in liquid nitrogen. Cells were subsequently lysed in a buffer composed of 20 mM Tris pH 7.5, 150 mM NaCl, 1 mM EDTA, 1 mM EGTA, 0,1% NP40, Protease inhibitor cocktail 1x, RNAse Out 100 U/mL, and 400 µM VRC. The 35 strokes of Dounce homogenizer were applied to the sample before clarification at 5,000*g* for 5 min at 4°C. After preclearing using naked protein A-coated magnetic beads (Bio-Rad #161-4013), 2 µg of IgG control or anti-Staufen antibody (**Suppl. Table 3**) was mixed to 0.5 mg of lysates overnight under rotating incubation at 4°C. Beads were then added to complexes and incubated on a rotating wheel at 4°C for 2 h, then washed twice with lysis buffer. Twenty µg of total lysates 1/6th of the IP fraction, as well as flow-through fractions were loaded onto SDS-PAGE gels for subsequent immunodetection of the proteins of interest. Staufen-1-bound RNA extraction was conducted using the acid phenol approach detailed previously [8]. Bound RNAs were retrotranscribed using the Superscript IV Vilo RT enzyme (Invitrogen) and corresponding cDNAs were amplified using the Bioline No-Rox qPCR kit.

Filter binding assay

The *NTN1* 5'UTR was *in vitro* transcribed using the MEGAscript™ T7 Transcription Kit, (Ambion, #AMB13345) and then biotinylated (Pierce™ RNA 3' End Biotinylation Kit, Thermo #20160). HBV RNA epsilon loop was chemically synthesized and labeled (Genscript, Piscataway, USA). Sequences and genetic references are provided in **Suppl. Table 5.** RNA renaturation was performed by heating samples at 95°C for 5 min before slowly cooling to

room temperature. RNA constructs (0.1 nM) were then incubated with increasing concentrations of the purified recombinant Staufen-1 protein (Origen, #TP760787; 0-100 nM) in binding buffer (Tris-HCl, pH 7.4, 20 mM; K(AcO), 100 mM; KCl, 200 mM; $Mg(AcO)_2$, 2.5 mM; DTT, 1 mM) for 30 min at 37 °C. The reactions were then loaded onto a filter sandwich composed of 0.45 µm nitrocellulose filters (GE Healthcare Life Science) located above nylon filters (GE Healthcare Life Science). Both membranes were pre-soaked in binding buffer and assembled in a dot-blot apparatus. Samples were directly added to the filters under vacuum and subsequently washed twice with 400 µL of ice-cold binding buffer while a vacuum was being applied. Both membranes were then UV crosslinked (0.12 J/cm^2). Signal development was performed using the Chemiluminescent Nucleic Acid Detection Module Kit, thermo #89880. Quantification of the obtained signals was done using Image Lab. Kd values were calculated using the Sigma Plot 8.02© software according to the equation $y = y0 + (B_{max} \cdot xn)/(K_d^n + x^n)$, where y is the percentage of complexed RNA, Bmax is the binding yield, x is the concentration of the target RNA, Kd is the dissociation constant and n is the Hill coefficient.

RUSH assay

HepaRG cells transfected with a GFP-tagged A_1AT RUSH reporter described previously [36] were treated or not with poly(I:C). After 72 h, cells were treated with 40 µM biotin and then fixed with 3% paraformaldehyde at different time points. After immunofluorescence staining, images were acquired on a Leica SP5 confocal laser scanning microscope using the 63× oil objective at two-fold magnification.

Netrin-1 Crispr cell lines

A netrin KO Crispr cell line and its ad hoc control cell line were generated.

The Zhang lab protocol [37] was used. Briefly, guide sequences (**Suppl. Table 6**) were inserted into lentiCRISPR v2 (Addgene plasmid #52961) and lentiCRISPR v2-Blast (Addgene plasmid #83480). DNAs (Gag-Pol + Env + lentiCRISPRv2 or lentiCRISPRv2 Blast) were transfected into 2 × 10^6 HEK293T cells (ATCC CRL-1573) seeded the day before in 10-cm plates using calcium phosphate [38]. The medium (8 mL/plate) was replaced 16hrs after transfection. Virus-containing supernatants were harvested 24 h later, filtered through 0.45-µm pore-sized membranes, and stored at -80°C until further transduction. For selection of the resulting polyclonal cell lines, cells were plated at a density of 4.10^4/cm^2 in a 35 mm Petri dish. The next day later, lentiviral transduction was done using 500 µL of medium to which were added 250 µL of each lentivirus supernatant, for two days. Cells were then put under selective pressure for the expression of both lentiviruses' cassettes using puromycin and blasticidin (Invivogen, gradually increasing concentrations from 4 and 8 µg/mL to 10 and 20 µg/mL within

two weeks, comprising two weekly trypsinization procedures). Cell lysates were then generated for netrin-1 KO monitoring by Western blot using the anti-netrin-1 reference Ab126729 (Abcam) prior to liquid nitrogen storage.

Netrin-1 release assay

For netrin-1 release assays, Crispr control (HepaRG-Ctrl-KO) and netrin-1 KO (HepaRG-Net-KO#3) cell lines were seeded as depicted above, allowed to reach confluency for 4 days, and sequentially treated with recombinant soluble netrin-1 (125 ng/mL, R&D systems) followed by 50 µg/mL poly(I:C) for the indicated times, before supernatant harvesting and its clarification (1,000*g*, 5 min, 4°C). Supernatants were washed with ice-cold PBS and processed for netrin-1 immunoprecipitation and Western blotting.

Results

Clinical and *in vivo* relevance of netrin-1 induction

In order to evaluate the clinical likelihood of an interplay between netrin-1 and inflammation in the liver, we first considered a potential association between netrin-1 and clinical activity scores, performing western blotting (after extensive anti-netrin-1 antibody validation, **see Suppl. Fig.1**) on a well characterized HBV-positive series of samples. Samples were selected based on several criteria in order to minimize confounding factors, namely gender (men only here due to availability), similar HBV sample-specific viral loads, fibrosis scores, platelet counts, prothrombin time, ALAT, albumin and bilirubin, leading to a cohort of 14 patients **(Suppl. Table 1)**, the sample sizes of whom were compatible with multitarget immunoblotting. Samples were blotted for netrin-1 and α-SMA, an inflammation-related marker in CLDs [39, 40], and association between netrin-1 signals and activity were observed (**Fig.1A**), being however uncorrelated with corresponding netrin-1 mRNA signals **(Fig.1B and Suppl. Fig.3).** Based on activity scores, such data suggest that netrin-1 protein levels are correlated with liver inflammation in HBV patients.

In order to probe the robustness of these correlative clinical data, we first investigated the potential impact of experimentally-induced inflammation, using a panel of TLR ligands, namely Pam3-CSK4 as a TLR1/2 agonist, lipopolysaccharide (LPS) as a TLR4 agonist, FLA as a TLR5 agonist, FSL as a TLR2/6 agonist, Riboxol (molecularly defined TLR3 agonist), and finally low or high molecular weight poly(I:C) as TLR3, RIG-I and MDA-5 agonists. Experiments were carried out on HepaRG cells as a source of essentially growth-arrested and untransformed cells representative of late-stage CLD [41, 42]. RIG-I was also probed as a control for the induction of inflammation. Pam3CSK4, LPS, FSL, Riboxol, and HMW poly(I:C) induced netrin-1, suggesting its broad spectrum of inflammation triggers, and therefore its relevance, in the hepatic environment (**Fig. 1C**). Chronic viral infections of the liver represent one of the major etiologies of CLDs. Both HBV and HCV viruses have been shown to be direct inducers of dsRNA-based responses [43, 44], which in turn unleash the subsequent inflammation in hepatocytes. HepaRG cells were previously shown to be broadly responsive to poly(I:C) [45]. We hereafter focused on the dsRNA analog poly(I:C) of HMW, as a viral mimetic.

We then assayed inflammation-related netrin-1 induction in the liver *in vivo*. To achieve this, C57BL/6J mice of both sexes were challenged with HMW-poly(I:C), prior to harvesting their liver, and processing total RNA extracts for RT-qPCR on inflammation-related transcripts. Although poly(I:C) injection did not increase ALT levels (a well-known marker of liver inflammation) in mouse serum within the experimental timeframe (**Suppl Fig.4A**), several other markers of inflammation (*CXCL10*, *IL1B*, *IL6*, *KC*) were induced both in male and female mice. Interestingly, the overall inducibility of canonical inflammation markers was higher in

females. (**Suppl. Fig. 4B**). Intriguingly, though *NTN1* mRNA induction was not observed within total RNA populations, a western blot and IHC approach evidenced netrin-1 induction at the protein level, albeit to different extents with female mice being also more responsive (**Fig. 1D-E** and **Suppl. Fig. 5**). Such data suggest a causal link between inflammation, inflammation intensity, and netrin-1 induction, at least in the acute inflammatory context. In order to identify the cells implicated in netrin-1 induction, we performed intrahepatic IHC to detect netrin-1 in these murine samples. Netrin-1 staining yielded a homogenous and likely ubiquitous expression pattern, similar to previous data obtained in human liver [9]. Therefore, it is likely that netrin-1 staining was associated with the hepatocytic compartment, which makes up 80% of the liver mass and areas (**Fig. 1F**).

Translational induction of netrin-1

To gain further insight into the mechanisms of netrin-1 production, we conducted a set of *in vitro* experiments using HepaRG cells [41] and PHH that present two distinct phenotypes (preneoplastic and fully differentiated, respectively), and are deemed relevant for studying CLD-related mechanisms in untransformed hepatocytic cells. In HepaRG and PHH, poly(I:C) led to netrin-1 protein induction in a dose- and time-dependent manner. The RIG-I inducible marker was monitored to verify poly(I:C) activity. (**Fig. 2A**). As a laminin-related protein [46], netrin-1 is susceptible to be secreted and may also accumulate at the extracellular side of the plasma membrane. We thus tested netrin-1 signals by immunoprecipitation after heparin-based release of plasma membrane-bound netrin-1 in serum-free culture supernatants. Data indicate that the previously observed netrin-1 upregulation by Western blot affects its membrane-bound form along with its presence in the culture medium in both cell types **(Fig. 2B)**. We then ascertained that its upregulation was independent of its well-documented activity as a cell death inducer. We thus monitored cell viability upon poly(I:C) and heparin treatment, using the neutral red assay in wild-type HepaRG, PHH, and Crispr/Cas9 netrin-1 KO HepaRGs **(Suppl. Fig. 6A-C)**. Previous data were confirmed, indicating that during inflammation, netrin-1 induction is not related to cell injury and is likely involved in cell death-unrelated processes.
We next sought to unravel the molecular basis for netrin-1 induction. Similarly to mice, no significant increase in *NTN1* mRNA levels could be evidenced, either in HepaRG cells or in PHH (**Suppl. Fig. 7A**), upon analysis of total RNA pools. Total RNA levels for a given mature transcript depend on various processes that are active in real time, such as transcription, stability, and splicing. We initially focused on pre-mRNA levels, though no significant induction could be observed under poly(I:C) treatment in HepaRG or in PHH (**Suppl. Fig. 7B**). In order to rule out transcriptional induction in such contexts, we then performed a *Ntn1* promoter Luc reporter assay and a run-on assay aiming at quantifying *de novo NTN1* transcription under poly(I:C) treatment. No increase could be obtained following treatment of HepaRG cells with

poly(I:C), in either approach, indicating that netrin-1 was not regulated at the transcriptional level (**Suppl. Fig. 8A-B**).

To evaluate the possible implication of *NTN1* mRNA splicing in the final phenotype, we calculated the evolution of *NTN1* pre-mRNA over mRNA induction ratios upon poly(I:C) treatment. Again, no significant alteration of such ratios was observed (**Suppl. Fig. 9**), suggesting that regulation of splicing did not participate in netrin-1 protein increase. In order to safely orient subsequent studies towards post-transcriptional read-outs, we lastly quantified *NTN1* mRNA stability using the selective RNA polymerase II inhibitor triptolide [47]. In this assay, *NTN1* mRNA decay rate was unaltered (-1.3-fold) by poly(I:C) (**Suppl. Fig. 10**), arguing in favor of a post-transcriptional regulation.

Following the next step in the biogenetic processing of netrin-1, we then considered translational regulation as a potential contributor to netrin-1 protein induction. We first submitted HepaRGs, PHHs and mouse livers to total polysomal fractionation using sucrose gradient-based isopycnic ultracentrifugation followed by gradient trace monitoring, RNA extraction, and RT-qPCR on the *NTN1* transcript. Adequate fractionation could be evidenced using gradient UV traces. The presence of the peak of free messenger ribonucleoparticles (mRNPs), followed by the 40S, 60S and 80S ribosomal subunits, themselves finally followed by the typical oscillating profile of successive polyribosomes was delineated (**Fig. 3A,** black and red traces). As expected, translation was more active in early confluent HepaRG cells (as previously depicted [48]) than in resting, optimally differentiated, PHH, or mouse livers. Moreover, for HepaRG cells, the percentage of polysome-bound *NTN1* mRNA signals versus total *NTN1* signals remained unchanged upon poly(I:C) treatment (87.9% versus 86.0% in treated cells), whereas in PHH, a major shift of the *NTN1* signal could be observed towards the polysomal compartment of the gradient (46% versus 89%, $p < 0.05$) **(Fig. 3B-C)**. The absence of changes in mouse livers is concomitant to higher amounts of *NTN1* in heavy polysomes (fractions 13-17), that are associated with strong translational activity. In order to confirm this, an EDTA release control experiment was carried out. EDTA induces polysomal collapse through Mg^{2+} and Ca^{2+} chelation, enabling the evaluation of the genuine polysomal origin of the RT-qPCR signals, and reinforced these results (**Fig. 3A-C**).

Altogether, our data advocate for distinct modes of regulation of netrin-1 induction in HepaRG hepatocyte-like cells and fully differentiated environments such as PHH and mice livers. Mouse livers and PHH appear to activate total polysome-based translation of the *NTN1* transcript for the final induction of the protein. Yet, netrin-1 biogenesis mechanisms remain uncharted at this stage of the study in HepaRG cells, which are representative of late stage, preneoplastic, CLD.

In order to pursue the identification of the molecular basis of netrin-1 increase upon poly(I:C) treatment in HepaRG cells, the *de novo* incorporation of labeled amino acids into the netrin-1

sequence was quantified by MS after netrin-1 immunoprecipitation, using stable isotope labeling by amino acids in cell culture (SILAC) method. This SILAC approach indicated a 4.5-fold increase in *de novo* incorporation of amino acids in inflammatory conditions versus naïve cells (**Fig.3D-E**). These data suggest that if translation *per se* is not modulated in HepaRG cells, as found by polysomal fractionation, processes increasing the susceptibility of the *NTN1* transcript to translation are strong candidates.

Staufen-1 mediates netrin-1 induction through direct interactions with the *NTN1* transcript in preneoplastic cells

A majority of the transcriptome encoding secretory and membrane proteins is ER-bound [49]. Netrin-1 is a secreted protein and its translation should naturally take place in association with the endoplasmic reticulum (ER) membranes so that co-translational translocation of the nascent peptide across the ER membrane may occur through the transient association of the peptide's signal sequence with the translocon [50]. Therefore, netrin-1 translation is conditioned by two distinct events: association with polyribosomes and accumulation of the transcript at the ER level for subsequent transfer of the native peptide to the secretory pathway. We took into consideration this process in order to determine divergences between HepaRG cells and PHH for netrin-1 induction. Based on the so-called 'sequential extraction' method [32, 33], which allows the investigation of mRNA partitioning between cytosol and microsomes, we verified netrin-1 enrichment following poly(I:C) treatment using three protein markers (RIG-I and caspase-3 as cytosolic proteins and the ER-associated PDI/P4HD protein, **Fig. 4A**). Whereas no significant alteration in cytosolic or membrane-bound levels of *NTN1* transcripts was evidenced upon poly(I:C) treatment in PHH, the level of *NTN1* transcript enrichment in membrane-bound versus cytosolic fractions increased by 7-fold in inflammatory HepaRG cells ($p < 0.05$; **Fig. 4B)**. These finding indicate that translational induction of netrin-1 occurs via the transfer of the *NTN1* transcript to the ER prior to its active translation in HepaRG cells.

We then focused on *NTN1* mRNA relocalization by conducting a bibliographic search for proteins participating in transport and translational regulation of highly structured, GC-rich, mRNAs in their 5' ends, which the *NTN1* transcript belongs to [16]. The double-stranded RNA binding domain-containing protein Staufen-1 (STAU1) shuttles between the cytosol and the ER thanks to its association with microtubules through its tubulin binding domain [51, 52]. STAU1 is implicated in translational activation of GC-rich, structured, mRNAs 5'UTRs [53], and was shown to bind to the *NTN1* transcript in high throughput experiments [54, 55].

In resting cells, STAU1 displayed a granular staining also observed in other studies, where it associates with RNA granules before or after movement on microtubules [56-59]. Interestingly, poly(I:C) triggered the reconfiguration of STAU1 signals from a granular to a microtubule-like filamentous pattern, in accordance with other studies [51, 52, 56]. The number of STAU1-

positive granular foci per cell decreased 11-fold and the percentage of STAU1 filamentous staining-positive cells increased 9-fold with poly(I:C) (**Fig.5A-B**). STAU1 staining also displayed an increased overlap with PDI+ (ER) areas, quantified using the Li colocalization coefficient. (**Fig. 5C-D**)

In order to test direct interactions between Staufen-1 and the full length netrin-1 mRNA in our biological setting, we set-up a CLIP assay in UV cross-linked HepaRG cells using a variety of relevant negative and positive control transcripts [54, 55]. Immunoprecipitation conditions for STAU1 were first defined (**Fig. 6A**). Data depicted in this panel show significant increase in *NTN1* levels versus several other transcripts, in addition to a specific and positive impact of poly(I:C) *per se* on *NTN1* binding levels to STAU1. Percentages of transcript inputs are indicated in poly(I:C)-treated or untreated conditions in **Fig. 6B**.

To further probe such interactions, we carried out a filter binding assay, which provides information on the affinity of both partners and their class of interaction dynamics downstream of collected STAU1-bound, RNA-conjugated, biotin-avidin-HRP signals. Based on obtained profiles, filter binding data were fit to a sigmoidal equation to determine binding constants and to estimate the degree of binding cooperativity. Calculation of Kd led to a value of 1.17+/-0.11 nM. Calculation of the Hill constant was done using the previously published formula: Log (81) / Log (EC_{50}/EC_{10}) [60] and led to a value of 1.9+/-0.28, suggesting a moderately cooperative interaction. As a control, no interaction between an HBV epsilon loop RNA sequence and STAU1 was observed. In competition experiments, incubation of increasing concentrations of unlabeled *NTN1* 5'UTR led to displacement of the pre-bound labeled RNA as expected, while, again, no reversion of STAU1-NTN1 5'UTR complex-derived signals could be achieved using HBV control RNA **Fig.6C-D.** Altogether, such data suggest that the dsRNA binding protein STAU1 directly binds to the 5'UTR of the netrin-1 transcript, corroborating the accumulation of STAU1 at the ER level for enhanced susceptibility of this secreted protein's mRNA to translation upon poly(I:C) treatment.

In order to unequivocally test the functional implication of STAU1 in the accumulation of the *NTN1* transcript at ER sites for netrin-1 protein induction, we tested the effect of RNAi-mediated STAU1 depletion on poly(I:C)-induced *NTN1* accumulation at the ER and on netrin-1 induction. Both approaches showed reversion of poly(I:C)-induced netrin-1 signals **(Fig. 6E-G)**. Moreover, these mechanistic data indicated that Staufen-1-dependent transcript transfer to the ER in non-differentiated cells (here represented by proliferative HepaRG cells), determined netrin-1 induction *in vitro*. They represent to our knowledge the first functional description of Staufen-1 in inflammation. A comparison of results obtained in HepaRG cells and PHH suggests that mRNA relocalization and translational activation seem to be mutually exclusive mechanisms across both cell environments, yet converging and enabling netrin-1 induction.

Netrin-1 induction is unrelated to post-translational steps

In order to potentially define RNA relocalization as a unique contributor to netrin-1 upregulation during inflammation, the susceptibility of netrin-1 to enhanced secretion as well as its stability were considered downstream of this experiment. The hepatocyte is one of the major secretory cells of the human body. Since inflammation is also potentially regulated at the secretion level because of its important cytokinic component, we considered a potential impact of poly(I:C) treatment on cell secretion, which could itself regulate netrin-1 levels downstream of translation. Using the so-called RUSH (retention using selective hooks) assay [36] we treated or not HepaRG cells with poly(I:C) and, using immunofluorescence, we examined the ability of a fluorescent fusion form of alpha1-antitrypsin (AAT-GFP) to reach the Golgi apparatus (located using giantin staining) within the assay timeframe. As shown in **Suppl. Fig. 11A-B**, no noticeable difference was observed between colocalized signals derived from GFP or giantin in treated versus untreated cells. AAT being one of the most abundant and specific cargoes of the hepatocyte, such data suggest that the global secretory activity levels of HepaRG cells are not altered by poly(I:C), and that netrin-1 levels remain unaffected by this regulatory step.

To rule out the accumulation of netrin-1 through protein stability enhancement, we stopped translation by cycloheximide treatment prior to harvesting poly(I:C)-treated HepaRGs and PHH in a time-course assay and combined immunoprecipitation of cell-bound and secreted netrin-1. In these conditions, no alteration of netrin-1 protein decay rate could be evidenced (**Suppl. Fig. 12**). In association with previous data, these two last datasets provide final evidence that netrin-1 induction occurs through transcript localization regulation (undifferentiated HepaRGs) and translational activation (PHHs).

Induction mechanistics are constrained by the pathogenic status of origin of the cells

While HepaRG cells are capable of undergoing partial experimental hepatocytic re-differentiation under defined culture conditions, their pre-neoplastic status is established by their peritumoral origin in a cirrhotic liver [41]. In order to control netrin-1 induction mechanisms between HepaRG and PHH for the former's pathological origin, we submitted HepaRG cells to their usual hepatocytic differentiation protocol [42]. In polarized, quiescent and differentiated HepaRG, of note again, no *NTN1* induction occurred at the total RNA level in a context where netrin-1 protein is induced by poly(I:C). Yet, netrin-1 protein induction correlated with accumulation of *NTN1* mRNA in the membrane-bound compartment (**Suppl. Fig. 13**), as was the case with undifferentiated HepaRGs. This dataset indicates that the nature of post-transcriptional processes converging to netrin-1 induction is more constrained by the

pathological status of origin of the cells with respect to pre-neoplastic (HepaRG) or physiological (PHH) hepatic contexts than by their level of differentiation

A phase 2 trial-validated antibody enabling netrin-1 capture dampens inflammation in mice

As published in several studies, tissular inflammation may be altered by netrin-1 [20-22, 61] suggesting its mobilization in interstitial fluids. To test whether netrin-1 may act as an auto/paracrine factor with diffusible consequences, we monitored the behavior of exogenously added in-house validated recombinant netrin-1 [9], on netrin-1 KO Crispr cells upon poly(I:C) treatment. Using netrin-1 immunoprecipitation and Western blot, we observed that poly(I:C) mobilized netrin-1 within 2 hours from its cell-associated pool towards supernatants (**Suppl. Fig. 14)**, hence arguing in favor of its regulatory role in hepatic inflammation at the microenvironmental level.

Considering that this diffusible status corroborated previously known tissular effects of netrin-1 [20-22, 61], we treated C57BL/6J mice with the clinically used and well tolerated anti-netrin-1 antibody NP137 (NCT02977195) [27] or its NP001 isotypic control 32h before challenging them with poly(I:C) for 16h and liver harvest. Treatment with the former did dampen poly(I:C)-induced netrin-1 induction (**Fig.7A**), that occurred, again, independently of *NTN1* RNA upregulation in all instances (**Fig.7B**). RT-qPCR conducted on a panel of inflammation-related cytokines (*CCL2, CXCL10, IL1B, IL6, KC* (ortholog of human IL8), *IL12B, IL15,* and *TGFB1* highlighted a causal relationship between netrin-1 inactivation and reversion of the induction of several of these cytokines (*CCL2, CXCL10, IL1B, KC*, and *TGFB1,* **Fig. 7B**). In order to further document this phenotype, we performed a flow cytometry analysis to monitor immune cell population regulation. Gating strategies are shown in **Suppl. Fig.15**, where the three left panels depict $Ly6C^{+}$ $CD11^{low}$ $F4/80^{hi}$ gating (from top to bottom: Poly(I:C)+ and NP001, Poly(I:C)+ and NP137, and finally Ly6C FMO on pooled cells from all mice). Monocyte-derived macrophages ($CD45^{+}$ $CD11b^{+}$ $F4/80^{low}$) remained stable. Total Kupffer cells ($CD45^{+}$ $CD11b^{low}$ $F4/80^{hi}$) counts were not regulated. However, the NP137 antibody reversed $Ly6C^{+}$ Kupffer cells counts. (**Fig.7C**). Hence, such data suggest that netrin-1 is an actionable target that further amplifies dsRNA-triggered liver inflammation, in accordance with its role in other organs 1 [20-22].

Discussion

Netrin-1 has been repeatedly identified as a cancer promoting agent [5, 6, 10-15]. Its expression is associated with inflammatory diseases that may themselves promote cancer onset [6, 26]. Given the causal link between inflammation, cirrhosis, and HCC [62-66], probing the direct impact of inflammation on netrin-1 expression in the liver was of interest.

Although transcriptional regulation has been considered a hallmark regulatory step in general cell biology and liver differentiation processes [67], increasing evidence suggests that processes that need swift temporal regulation in highly remodeled tissues, such as inflammation and, more generally, oncogenic processes and associated resistance, rely on translational modulation [68, 69].

Our experience in the liver field has been recurrently confronted with this type of regulation. Indeed, differentiation of HepaRG cells is strongly associated with important downregulation of a majority of transcripts at the total RNA level, together with a concomitant upregulation in polysomal fractions of a subset of hepatocytic differentiation-related mRNAs [70]. Experimental activation of the mTOR/S6 kinase pathway, which is present in 45% of HCC cases [71], impairs hepatocytic differentiation, and impedes the translation of transcripts moderating lipid homeostasis and cell growth [31]. Upon the UPR, netrin-1 translation is selectively favored during global translational shut down, together with IRES-bearing transcripts implicated in cell survival and transformation [72]. Finally, the netrin-1 receptor UNC5-A is also translationally down-regulated upon HCV infection, including in patient livers [8]. Moreover, the liver is one, if not the most, active secretory and metabolic cell type in human physiology, in line with being exposed to real-time needs for metabolic and hence secretory regulation (acute phase, post-prandial phases). It is thus conceivable that the biogenesis of secreted factors such as netrin-1 are more often constrained by swift regulatory processes such as translational control in the liver than in other cell types. The present data, to be interpreted as a confirmation of the particular susceptibility of netrin-1 to post-transcriptional regulation, strengthens the need for more frequent molecular analyses of pathogenic processes using total RNA-unrelated enrichment methods, such as polysomal profiling, at least at the liver level.

In the present study, we have shown, depending on the cell system of interest, *i.e.* undifferentiated HepaRG or PHH, that netrin-1 biogenesis under inflammation was specifically regulated at the mRNA localization level in the former, while at the translational level *per se* in the latter case and that the pathogenic status of the cells conditioned these modes of induction. The presence of these mechanisms is of interest, since it appears that two distinct modes of post-transcriptional regulation actually converge towards a single phenotypic outcome, i.e., netrin-1 increase. Pathophysiological needs for delivering this final phenotype therefore seems

to override cell type-specific functional singularities, suggesting that induced netrin-1 conveys important functions in the liver, either immunomodulatory [20-22, 61], or, on the long-term, hepatoprotective as an anti-apoptotic factor [5, 6, 10-15].

This phenotype relies on the RNA-binding protein Staufen-1, the implication of which is to date essentially undocumented in the regulation of inflammatory processes. However, Staufen-1 has recently been shown to foster gastric cancer progression in a cyclin-dependent kinase-dependent manner [73] and also to take part in an EZH2-related, HCC promoting pathway [74], suggesting relevance of further studies aiming at characterizing its implication in end-stage liver disease through a possible netrin-1 involving axis.

From a more pathology- and therapy-oriented point of view, this study suggests a potential link between hepatic inflammation and liver disease progression through netrin-1. To date, in the liver, direct cross-talks between inflammation and HCC have been mainly defined through the IL-6/gp130/STAT3 axis [75]. We previously documented that progression towards HCC is associated with a sharp drop in *UNC5A* (netrin-1 receptors) expression levels [8], thereby functionally augmenting netrin-1 activity, following the dependence receptor theory [76]. Our study improves the understanding of the potential implication of inflammation in the evolution of CLDs, besides the well characterized IL-6/gp130/STAT3 cascade and identifies an actionable target for its modulation. Chronic inflammation of a given tissue is counterbalanced by a wound healing process leading to scar, acellular, tissue build up, made of ECM. As mentioned before, netrin-1 is a laminin-related protein that shares several structural features with ECM-constituting proteins. As a consequence, one may hypothesize that netrin-1 could participate in ECM build-up. The fact that netrin-1 promotes fibrosis in the inflammatory lung [77] strengthens the potential relevance of this hypothesis.

The humanized anti-netrin capture antibody NP137 developed by the authors [27] is currently under investigation in phase 2 clinical trials in general oncology (US Clinical Trials #02977195) and shows no clinical toxicity in a diversity of solid tumors contexts. The apparent anti-inflammatory activity of this antibody in the present setting argues in favor of its eventual transfer to the clinic for subsequent trials in histologically evolutive CLDs.

Acknowledgements

We thank B Bancel (pathologist, Lyon U. Hospital) for determining the activity scores, L Muller for technical assistance, A Paradisi for the netrin-1 promoter reporter plasmid, the CIQLE platform for assistance with confocal microscopy, and B. Manship for editing. RB and IC are recipients of a DevWeCan Labex (Laboratories of Excellence Network, ANR-LABX-061) and ANRS (ECTZ63958) predoctoral fellowships, respectively. Funding has been obtained through the same Labex consortium (ANR-LABX-061) and the French NCI (Inca PRT-K 19-033). Proteomic experiments were partially supported by the French NRA under projects ProFI

(Proteomics French Infrastructure, ANR-10-INBS-08) and GRAL, a program from the Chemistry Biology Health (CBH) Graduate School of University Grenoble Alpes (ANR-17-EURE-0003).

641 **Figure legends**

642

643 **Figure 1**

644 **Netrin-1 levels are correlated with activity scores in HBV-positive clinical liver**
645 **specimens, induced in HepaRG cells by several TLR ligands and induced by poly(I:C)**
646 **in mouse livers.**

647 **A**. HBV-infected liver tissues (clinico-biological features listed in supplementary table 1) were
648 homogenized using a Dounce homogenizer in lysis buffer, centrifuged to remove debris,
649 denatured, and visualized by SDS-PAGE. Netrin-1 and α-SMA were probed using antibodies
650 listed in **Suppl. Table 2**. Since actin staining is not correlated with the amount loaded, Ponceau
651 staining is shown as well. **B**. Corresponding RNA data are plotted versus activity scores. **C**.
652 Netrin-1 expression levels were evaluated by immunoblotting (n = 3 independent experiments).
653 RIG-I was used as a poly(I:C) activity control. **D**. The levels of *NTN1* mRNA were quantified
654 by RT-qPCR using *GUS* [78] as an internal reference. Mann-Whitney test (n.s.). **E**. Netrin-1
655 expression levels were evaluated by immunoblotting using anti-RIG-I and anti-netrin-1
656 antibodies. **F**. Liver slides were probed with the same anti-netrin-1 antibody prior to secondary
657 antibody incubation and HRP-based visualization. Mouse samples were derived from the same
658 hepatic lobe in all instances. Data are representative of a total of 40 mice (10 females, 10
659 males, +/- poly(I:C); **see Suppl. Fig. 4** for comprehensive data).

660

661 **Figure 2.**

662 **Cell-associated and soluble netrin-1 levels are upregulated by poly(I:C) in a time- and**
663 **dose-dependent manner in HepaRG cells and in PHH.**

664 **A**. Netrin-1 expression levels were evaluated by immunoblotting using an anti-netrin-1 antibody
665 (n = 3, HepaRG; and n = 3 distinct PHH batches). RIG-I was used as a poly(I:C) activity control.
666 **B**. Netrin-1 expression levels were evaluated by immunoblotting in total cell lysates or after
667 immunoprecipitation in supernatants, with or without heparin. NP001: isotype control. NP137:
668 anti-netrin-1 Ig. RIG-I was used as a poly(I:C) activity control.

669

670 **Figure 3.**

671 **Inflammation activates translation of the *NTN1* transcript in HepaRG cells, PHH and**
672 **mouse livers.**

673 HepaRGs, PHH and mouse livers samples were homogenized in polysome lysis buffer and
674 loaded onto a linear sucrose gradient prior to isopycnic ultracentrifugation. **A**. Representative
675 profile of UV gradient traces. **B**. *NTN1* distribution profile across the gradient. Total
676 polyribosomes were fractionated, extracted and processed for *NTN1* by RT-qPCR (n = 3,
677 HepaRG; n = 3 distinct PHH donors, n = 6 female mice). Mann–Whitney test, * $p < 0.05$. **A-B**.

An EDTA release control assay was performed by adding EDTA to lysates immediately before ultracentrifugation (green values). **C.** Quantification of corresponding polysomal signals. **D.** Total lysates and supernatants derived from treated and control HepaRG cells previously adapted to dialyzed serum conditions for 14 days (and labeled with medium or heavy Lys or Arg isotopes supplemented in Lys/Arg-free William's E medium) were lysed with 5x lysis buffer and quantified for total protein amounts and mixed 1:1 prior to netrin-1 immunoprecipitation. **E.** Immunoprecipitated material was then run onto SDS-PAGE, submitted to tryptic digestion and subsequent isotope-specific mass spectrometry-based quantification (n = 3 independent experiments). The schematic diagram was drawn using the BioRender software. Mann-Whitney test, *** $p < 0.001$.

Figure 4

***NTN1* accumulates in membrane/ER-positive fractions upon poly(I:C) treatment in HepaRG cells.**

The Stephens et al. sequential extraction method was used as mentioned in the materials and methods section. **A**. Adequate partitioning was verified by Western blotting on PDI (internal membrane contents) and caspase-3 (cytosolic contents). RIG-I (cytosolic location) was also probed as a poly(I:C) activity control. Differential Ponceau Red staining profiles are shown. **B**. *NTN1* transcripts were monitored for their partitioning by RT-qPCR. Mann-Whitney test, * $p < 0.05$ (n = 3 (HepaRG), and n = 3 distinct PHH batches).

Figure 5

Poly(I:C) induces Staufen-1 relocalization and accumulation at endoplasmic reticulum, PDI-positive, sites.

A. Representative immunofluorescence-based localization of PDI (red) and Staufen-1 (green). Nuclei were counterstained with Hoechst 33342. **B.** Number of Stau1-positive dots per cell and percentage of fibrillar Stau1-positive cells versus total cells are shown under resting or poly(I:C)-treated conditions. Mann-Whitney test after Shapiro-Wilk test (* $p < 0.05$, n = 3 independent experiments). **C.** Li diagrams and Li coefficient calculations for PDI and Staufen-1 colocalization quantification, respectively. Pixels present on the left and right sides of the y-axis, i.e., associated with negative and positive staining amplitude values, indicate exclusion and colocalization, respectively. Li coefficients were calculated using the JACop plugin from the ImageJ software (http://rsb.info.nih.gov/ij/plugins/track/jacop.html). Twenty random fields were acquired per biological sample, totaling 300-400 cells analyzed for each biological sample in a given single experiment (n = 3 independent experiments). **D.** Statistical assessment of the colocalization of PDI and Staufen-1. Red (PDI) and green (Stau1) fluorescence intensities were measured for each pixel along a 5µm line, using the Plot Profile

function of the ImageJ software. Spearman correlation coefficients for each couple of intensity values are indicated.

Figure 6

Staufen-1 interacts with *NTN1* mRNA through its 5'UTR, and conditions *NTN1* transcript relocalization and netrin-1 induction in proliferative HepaRG

A. CLIP / Staufen-1 immunoprecipitation. HepaRG cell lysates derived from UV crosslinked monolayers were immunoprecipitated with naked, IgG control or anti-STAU1-coupled beads prior to elution and 1D SDS-PAGE. **B.** negative control (mitochondrial) transcripts, positive control [54] transcripts for STAU1 binding, and *NTN1* were quantified on immunoprecipitated materials relatively to inputs. Mann-Whitney test, *** $p < 0.01$ (n = 5 independent experiments). **C.** Filter binding assay. Biotin-labeled *NTN1* 5'UTR or HBV RNA epsilon loop at constant amounts were titrated for their ability to undergo trapping by the upper nitrocellulose membrane ('Nitro') or reach the lower nylon membrane ('N+') by increasing amounts of recombinant STAU1 protein. Corresponding quantification of HRP signals and obtained parameters are shown. **D**. Competition experiments using the filter assay approach. Pre-bound STAU1-*NTN1* 5'UTR biotin(+) complexes were submitted to increased concentrations of unlabeled competitors (*NTN1* 5'UTR or HBV epsilon RNAs) and processed on both membranes. Corresponding quantification of HRP signals and obtained parameters derived from one representative experiment because of variability are shown (n = 5 independent experiments). **E**. Impact of Staufen-1 depletion on netrin-1 induction was evaluated by immunoblotting. **F**. Adequate partitioning between cytosolic (C) and membrane (M) fractions was addressed by Western blotting on PDI (internal membrane contents) and caspase-3 (cytosolic contents). RIG-I (cytosolic location) was probed as a poly(I:C) activity and cytosolic control. **G**. *NTN1* was then quantified by RT-qPCR in both fractions. Mann-Whitney test, ** $p < 0.01$ (n = 3 independent experiments).

Figure 7

Netrin-1 capture by a clinically used antibody dampens hepatic inflammation in mice.

A. Hepatic netrin-1 levels were measured by western blotting. **B**. *NTN1* and indicated cytokines mRNAs levels were quantified by RT-qPCR using the *GUS* transcript as a reference. **C**. Percentage of positive live (DsRed) cells against CD45, CD11b, F4/80, Ly6C, CD3, CD8 and CD69 markers are indicated in the presence or absence of poly(I:C) and netrin-1 inactivation (n = 5-8 mice per group).

Figure 8

Netrin-1 is a pro-inflammatory factor up-regulated upon inflammation by exclusive translational activation or Staufen-1 dependent regulation processes in the liver.

Poly(I:C) drives netrin-1 upregulation in hepatocytes through translational activation or Staufen-1-mediated accumulation to the ER membrane. Poly(I:C) alters netrin-1 binding to the extracellular side of the membrane and potentiates its activity as a secreted soluble factor. Blocking netrin-1 signaling with NP137 reverses Kupffer cells activation and pro-inflammatory cytokine transcripts amounts in total liver extracts.

Supplementary Figure 1.

In-house assessment of anti-netrin-1 antibody staining reliability.

A-B. A panel of hepatocyte-like cell lysates derived from *NTN1* mRNA negative or positive cells was probed by RT-qPCR and netrin-1 Western blotting, respectively, using the Abcam reference Ab126729. **C-D**. Crispr/Cas-9 engineered netrin-1 KO HepaRG cells and *NTN1* siRNA-treated HEK293T cells, respectively, were subjected to anti-netrin-1 immunoblotting using the same antibody.

Supplementary Figure 2.

Sequential extraction method.

Phase contrast microscopy of sequential extraction steps are shown for HepaRG cells. **A.** After stripping the intact cells of their cytoplasm (left panel) and then of their internal membrane contents (center), only nuclei remain visible as attached to the plastic dish (right panel, **B**).

Supplementary Figure 3.

Netrin-1 protein levels and transcripts are not correlated in human liver tissues.

HBV-infected liver tissues (clinico-biological features listed in supplementary table 1) RNA data are stratified in a sample specific manner.

Supplementary Figure 4.

Poly(I:C) activity assessment in mice.

A. ALT activity was monitored in the serum of the same mice challenged with poly(I:C). n = 10 females and 10 males, +/- poly(I:C), corresponding to 40 animals. * $p < 0.05$, ** $p < 0.01$, Mann-Whitney test after Shapiro-Wilk test. ULN, upper limit of normal values. **B**. C57BL/6J mice were challenged with poly(I:C), their liver harvested, and total RNA extraction processed for RT-qPCR on inflammation-related transcripts. Corresponding canonical markers of inflammation activation (*IL1B*, *IL6*, *CXCL10, KC* (ortholog of h*IL8*)) were monitored.

Supplementary Figure 5.

Dot blot quantification of netrin-1 using in-house validated anti-netrin-1 antibody. **A.** Ponceau staining was used as a loading reference. N = 10 females and 10 males, +/- poly(I:C), corresponding to 40 animals.

Supplementary Figure 6.

Poly(I:C) does not alter cell viability in HepaRG and PHH.

Viability was quantified by the Neutral Red assay. **A.** n = 3 (HepaRG); n = 3 distinct PHH batches, **B.** n = 3 (Netrin-1-KO and control Crispr/Cas-9 HepaRG). Mann-Whitney test (n.s.). **C**. Cells were treated with heparin overnight prior to harvesting (HepaRG, n = 3, n.s).

Supplementary Figure 7.

***NTN1* total RNA and pmRNA levels are unaffected by poly(I:C) either in a time- or dose-dependent manner in HepaRG cells and in PHH.**

A. The levels of *NTN1* mRNA were quantified by RT-qPCR using *GUS* as an internal reference. Statistical significance was determined using the Mann-Whitney test. (n.s.). **B.** The levels of *NTN1* pre-mRNAs (intron 1) were quantified likewise. No amplification occurred when using heat-inactivated RT (green square). Mann-Whitney test (n.s.). n = 3 independent experiments (HepaRG); n = 3 distinct PHH donors run in technical triplicates.

Supplementary Figure 8.

***NTN1* transcription is not induced by poly(I:C) in HepaRG cells.**

A. The levels of *Ntn1* promoter-dependent Luciferase expression were evaluated using a *Ntn1* promoter (-1740; +1) Luc expressing plasmid. **B**. Quantification of *de novo* transcription of *NTN1* using a run-on assay. Mann-Whitney test (* $p < 0.05$).

Supplementary Figure 9

***NTN1* mRNA splicing remains unaffected by poly(I:C).**

A. *NTN1* mRNA over pmRNA ratios were calculated. Mann-Whitney test (n.s.). n = 3 independent experiments (HepaRG), and n = 3 distinct PHH batches run in technical triplicates.

Supplementary Figure 10

***NTN1* transcript stability is not regulated by poly(I:C).**

HepaRG cells were treated with poly(I:C) for 48hrs before adding the RNA polymerase II inhibitor triptolide to the medium and harvesting cells at different time points to quantify *NTN1* and *c-fos (FOS)* by RT-qPCR. **A.** Total mRNA integrity throughout the experimental time-course was monitored using the Bioanalyzer device. **B.** *c-fos* levels collapse was used as a

control for assessing triptolide activity. **C.** *NTN1* transcript decay rate in control and poly(I:C)-treated conditions was calculated. n = 3 independent experiments. Mann-Whitney test (n.s.).

Supplementary Figure 11

Poly(I:C) does not alter the functionality of the hepatocytic secretory pathway using A_1AT as a hepatocyte-specific major cargo.

A. HepaRG cells were transfected with A_1AT-GFP bearing plasmids in biotin-free medium and treated or not with poly(I:C). **B.** GFP and giantin colocalization were then estimated in a time course assay after the addition of biotin to the medium (means of n = 2 independent experiments are shown). Mann-Whitney test (n.s.).

Supplementary Figure 12

Netrin-1 protein stability is not modified by poly(I:C)

Cells were treated by poly(I:C) for 48 hours and with cycloheximide at 48 hours to stop translation. **A.** Cells and supernatants were then harvested and total netrin-1 pools immunoprecipitated before immunoblotting with netrin-1 antibody. **B.** Densitometry was performed to evaluate protein amounts (n = 6 independent experiments).

Supplementary Figure 13

Netrin-1 induction in differentiated HepaRG cells relies on relocalization of the *NTN1* transcript.

A. Netrin-1 expression levels were evaluated by immunoblotting using an anti-netrin-1 antibody. Inflammation induction was verified using anti-RIG-I antibody. **B**. *NTN1* expression levels were quantified by RT-qPCR. Mann-Whitney test (n.s.). **C**. Differentiated HepaRG were treated with cycloheximide, scraped, lysed and loaded atop of a linear sucrose gradient prior to isopycnic ultracentrifugation. Representative profile of UV gradient traces is shown. **D**. *NTN1* distribution profile across the gradient was identified by RT-qPCR. **C-D.** An EDTA release control assay was performed by adding EDTA to lysates immediately before ultracentrifugation (green values). **E**. Percentages of polysomal *NTN1* transcripts versus total are shown (n = 3). Mann-Whitney test (n.s.). **F**. Adequate partitioning was addressed by western blotting on PDI (internal membrane contents) and caspase-3 (cytosolic contents). RIG-I (cytosolic location) was probed as a poly(I:C) activity control. **G**. *NTN1* transcripts were monitored for their partitioning by RT-qPCR. Mann-Whitney test, * $p < 0.05$. (All data shown derive from n = 3 independent experiments).

Supplementary Figure 14

Inflammation mobilizes netrin-1 from its cell-associated pool.

Netrin-1 KO Crispr/Cas9 HepaRG cells were pretreated with recombinant netrin-1 (previously in-house validated for activity [9]) for 4 hours, and subsequently incubated with poly(I:C). for the indicated times. Cells were then submitted to total lysates- and IP-based immunoblotting for RIG-I as a poly(I:C) activity control and netrin-1. Tubulin and Ponceau staining were performed to ascertain purity of extracellular IP material. One experiment out of three is shown.

Supplementary Figure 15

Gating strategy for FACS experiment on mouse livers.

Live cells singlets of interest were gated prior to CD45+ sorting. Monocyte-derived macrophages are $CD45^{+}$ $CD11b^{+}$ $Ly6G^{-}$ $F4/80^{lo}$. Kupffer cells are $CD45^{+}$ $CD11b^{lo}$ $Ly6G^{-}$ $F4/80^{hi}$, and $Ly6C^{+}$ when pro-inflammatory.

Suppl. Table 1. Clinico-biological features of clinical samples

A.

	median (range)
N	14
Sex	men
age	68 (41 -83)
etiology	HBV
HBV RNA (copy / mL)	2,281,132 (1,958 - 1,215,827,224)
Metavir activity (A0)	3
Metavir activity (A1)	9
Metavir activity (A2)	2
Metavir fibrosis (F4)	14
Platelets counts (x10^3/mL)	124 (15-225)
Albumin (g/L)	37 (26-45)
ALAT (IU/mL)	67 (22-110)
TP (%)	77 (16-100)
Bilirubin (microM)	14 (6-291)

B.

	Activity score		
	A0	A1	A2
N	3	9	2
Sex	men	men	men
age	58 (42-75)	67 (40-83)	76 (71- 82)
etiology	HBV	HBV	HBV
HBV RNA (copy / mL)	8,978,257 (5,441-267,278,693)	1,303,239 (5,283-1,215,827,224)	39,499,659 (1,958-78,997,360)
Metavir fibrosis (F4)	all F4	all F4	all F4
Platelets counts (x10^3/mL)	206 (187-225)	99 (15-178)	194 (172-216)
Albumin (g/L)	NC	36 (26-44)	45
ALAT (IU/mL)	48 (24-71)	72 (35-110)	29 (22-35)
TP (%)	79 (71-87)	75 (16-100)	93 (91-95)
Bilirubin (microM)	11,5 (11-12)	16 (6-291)	10

Suppl. Table 2. Antibodies

Antigen	Ig Species	Cat. Number & supplier	Antibody registry (RRID) #
Beta-actin	Mouse monoclonal	sc-8432, Santa Cruz	AB_626630

Beta-tubulin	Rabbitt polyclonal	Ab6046, Abcam	AB_2210370
Alpha-SMA	Rabbitt monoclonal	1924S, Cell signalling	AB_2734735
Netrin-1	Rabbit monoclonal	Ab126729, Abcam	AB_11131145
Netrin-1	Mouse monoclonal (humanized)	NP137, Netris Pharma	AB_2811180
RIG-I	Mouse monoclonal	sc-376845, Santa Cruz	AB_2732794
PDI (P4HB)	Mouse monoclonal	sc-74551, Santa Cruz	AB_2156462
PD1 (P4HB)	Rabbit monoclonal	Ab2792, Abcam	AB_303304
Caspase-3	Rabbit polyclonal	9662, Cell Signaling	AB_331439
CD11b	Rat IgG2b, κ	BLE101206	AB_215609
CD68	Rat IgG2a	BLE137029	N/A
F4/80	Rat IgG2a, κ	BLE123135	N/A
Ly6C	Rat IgG2c, κ	BLE128017	N/A
Ly6G	Rat IgGa, κ	BLE127613	AB_2573503
CD38	Rat IgG2a, κ	BLE102720	AB_10128557
Staufen-1	Rabbit polyclonal Mouse monoclonal	Ab73478, Abcam TA811475, Origene	AB_10712675 ND
Rabbitt isotype control	Rabbit IgG	Ab172730, Abcam	AB_2687931
Human isotype control	Mouse IgG1 (humanized)	NP001, Netris Pharma	N/A
Anti-mouse-HRP	Goat polyclonal	A4416, Sigma	AB_258167
Anti-Rabbit-HRP	Goat polyclonal	A6154, Sigma	AB_258284

Anti-rabbit-Alexa 488	Donkey polyclonal	A21206, Invitrogen	AB_2535792
Anti-mouse 594	Goat monoclonal	A11032, Invitrogen	AB_2534091

882

883 **Suppl. Table 3**

Target	**Reference**	**Provider**	**Cat. #**
N/A (Ctrl siRNA)	SiC001	Sigma	SiC001
STAU1	Si00734902	Qiagen	3407629
STAU1	Si04231584	Qiagen	3407629
STAU1	Si04269335	Qiagen	3407629
STAU1	Si04272387	Qiagen	3407629

884

885 **Suppl. Table 4. Human and mouse qPCR primers**

Gene symbol	**Genbank acc. #**	**Primer sequences (5'-3', F/R)**	**PCR conditions**	**Amplicon length, bp**
NTN1 (human)	NM_004822.3	CTTCTGCGGCAGGCGGACAGAT ACGCGTTGCAGAGGTGGCACGA	Denaturation, 95°C; annealing, 65°C, 3-step, 10% DMSO	385
NTN1 (human)	NM_004822.3 (pre mRNA)	GGTAAAGTCCCGAACGCGG AAGTTTCGGGCGCAGGAGAG	Denaturation, 95°C; annealing, 55°C	133
GUS (human)	NM_001293105	CGTGGTTGGAGAGCTCATTTGG AA TTCCCCAGCACTCTCGTCGGT	Denaturation, 95°C; annealing, 55°C	72
ND1 (human)	Mitochondrial DNA	CCCTACTTCTAACCTCCCTGTTC TTAT CATAGGAGGTGTATGAGTTGGTC GTA	Denaturation, 95°C; annealing, 60°C	82

ATP6 (human)	Mitochondrial DNA	CATTTACACCAACCACCCAACTATC CGAAAGCCTATAATCACTGTGCC	Denaturation, 95°C; annealing, 60°C	82
C11ORF58 (human)	NM_014267.6	GGACTTGGCTTCAGTGAGGT TCAGGTGAATCATCATCGTCA	Denaturation, 95°C; annealing, 60°C	86
MDM2 (human)	NM_002392.6	CATGCCTGCCCACTTTAGA GGAGGCTCCCAACTGCTT	Denaturation, 95°C; annealing, 60°C	62
NTN1 (mouse)	NM_008744.2	CCTGTCACCTCTGCAACTCT TGTGCGGGTTATTGAGGTCG	Denaturation, 95°C; annealing, 55°C	78
GUS (mouse)	NM_010368.1	GTGGTATGAACGGGAAGCAAT AACTGCATAATAATGGGCACTGT	Denaturation, 95°C; annealing, 55°C	97
IL6 (mouse)	NM_031168	TCTATACCACTTCACAAGTCGGA GAATTGCCATTGCACAACTCTTT	Denaturation, 95°C; annealing, 60°C	88
CXCL10 (mouse)	NM_021274	CAAAGTGCTGCCGTCATTTT CTCAACACGTGGGCAGGATA	Denaturation, 95°C; annealing, 60°C	177
CCL2 (mouse)	NM_011333	CAGTTAACGCCCCACTCACC ACAGCTTCTTTGGGACACCT	Denaturation, 95°C; annealing, 60°C	112
IL1B (mouse)	NM_008361	TGATGTGCTGCTGCGAGATT TGCCACCTTTTGACAGTGATG	Denaturation, 95°C;	138

			annealing, 60°C	
KC (mouse)	NM_008176.3	CCATGGCTGGGATTCACCTC CAAGGGAGCTTCAGGGTCAA	Denaturation, 95°C; annealing, 60°C	58
MIP2 (mouse)	NM_009140.2	GCAAACTTTTTGACCGCCCT TCCAGAGCTTGAGTGTGACG	Denaturation, 95°C; annealing, 60°C	86
IL12B (mouse)	NM_008352	TGGTTTGCCATCGTTTTGCTG ACAGGTGAGGTTCACTGTTTCT	Denaturation, 95°C; annealing, 60°C	60
IL15 (mouse)	NM_001254747.1	CATCCATCTCGTGCTACTTGTG GCCTCTGTTTTAGGGAGACCT	Denaturation, 95°C; annealing, 60°C	112
IL4 (mouse)	NM_021283	GGTCTCAACCCCCAGCTAGT GCCGATGATCTCTCTCAAGTGA T	Denaturation, 95°C; annealing, 60°C	102
IL10 (mouse)	NM_010548	GCTGGACAACATACTGCTAACC ATTTCCGATAAGGCTTGGCAA	Denaturation, 95°C; annealing, 60°C	78
TGFB (mouse)	NM_011577	GAGCCCGAAGCGGACTACTA TGGTTTTCTCATAGATGGCGTT G	Denaturation, 95°C; annealing, 60°C	82

Suppl. Table 5

NTN1 5'UTR sequence (NM_004822, GenBank acc. # NM_004822, 5'-3')

ACUCCCAGCGCGAGUGGCGGCGGCGGCGGAGCCUUCGGGGGCGAGCGCGCGUGU GUGUGAGUGCGCGCCGGCCAGCGCGCCUUCUGCGGCAGGCGGACAGAUCCUCGG CGCGGCAGGGCCGGGGCAAGCUGGACGCAGCAUGAUGCGCGCAGUGUGGGAGGC GCUGGCGGCGCUGGCGGCGGUGGCGUGCCUGGUGGGCGCGGUGCGCGGCGGGC CCGGGCUCAGCAUGUUCGCGGGCCAGGCGGCGCAGCCCGAUCCCUGCUCGGACG AGAACGGCCACCCGCGCCGCUGCAUCCCGGACUUUGUCAAUGCGGCCUUCGGCAA GGUU
HBV epsilon loop (Genotype ayw, GenBank acc. # NC_003977.2, 5'-3') CUUGUUCAUGUCCUACUGUUCAAGCCUCCAAGCUGUGCCUUGGGUGGCUUUGGG GCAUGGACAUCC

Suppl. Table 6

CRISPR_CTRL_NEG_guide1	GTATTACTGATATTGGTGGG	lentiCRISPRv2 Puro
CRISPR_CTRL_NEG_guide1	CCCACCAATATCAGTAATAC	
CRISPR_CTRL_NEG_guide2	CCATCACCGATCGTGAGCCT	lentiCRISVPv2 Blast
CRISPR_CTRL_NEG_guide2	AGGCTCACGATCGGTGATGG	

CRISPR_NTN1_target_guide1	CGAACGCGGACTTTCCGGCG	lentiCRISPRv2 Puro
CRISPR_NTN1_target_guide1	CGCCGGAAAGTCCGCGTTCG	
CRISPR_NTN1_target_guide2	GCGCGACTCGTACTTCTACG	lentiCRISVPv2 Blast
CRISPR_NTN1_target_guide2	CGTAGAAGTACGAGTCGCGC	

References

1. El-Serag HB. Epidemiology of viral hepatitis and hepatocellular carcinoma. Gastroenterology. 2012;142(6):1264-73 e1. Epub 2012/04/28. doi: 10.1053/j.gastro.2011.12.061. PubMed PMID: 22537432; PubMed Central PMCID: PMC3338949.
2. Lee UE, Friedman SL. Mechanisms of hepatic fibrogenesis. Best Pract Res Clin Gastroenterol. 2011;25(2):195-206. Epub 2011/04/19. doi: 10.1016/j.bpg.2011.02.005. PubMed PMID: 21497738; PubMed Central PMCID: PMC3079877.
3. Serafini T, Kennedy TE, Galko MJ, Mirzayan C, Jessell TM, Tessier-Lavigne M. The netrins define a family of axon outgrowth-promoting proteins homologous to C. elegans UNC-6. Cell. 1994;78(3):409-24. Epub 1994/08/12. PubMed PMID: 8062384.
4. Mazelin L, Bernet A, Bonod-Bidaud C, Pays L, Arnaud S, Gespach C, et al. Netrin-1 controls colorectal tumorigenesis by regulating apoptosis. Nature. 2004;431(7004):80-4. Epub 2004/09/03. doi: 10.1038/nature02788. PubMed PMID: 15343335.
5. Fitamant J, Guenebeaud C, Coissieux MM, Guix C, Treilleux I, Scoazec JY, et al. Netrin-1 expression confers a selective advantage for tumor cell survival in metastatic breast cancer. Proceedings of the National Academy of Sciences of the United States of America. 2008;105(12):4850-5. Epub 2008/03/21. doi: 10.1073/pnas.0709810105. PubMed PMID: 18353983; PubMed Central PMCID: PMC2290782.
6. Paradisi A, Maisse C, Bernet A, Coissieux MM, Maccarrone M, Scoazec JY, et al. NF-kappaB regulates netrin-1 expression and affects the conditional tumor suppressive activity of the netrin-1 receptors. Gastroenterology. 2008;135(4):1248-57. Epub 2008/08/12. doi: 10.1053/j.gastro.2008.06.080. PubMed PMID: 18692059.
7. Dumartin L, Quemener C, Laklai H, Herbert J, Bicknell R, Bousquet C, et al. Netrin-1 mediates early events in pancreatic adenocarcinoma progression, acting on tumor and endothelial cells. Gastroenterology. 2010;138(4):1595-606, 606 e1-8. Epub 2010/01/19. doi: 10.1053/j.gastro.2009.12.061. PubMed PMID: 20080097.
8. Plissonnier ML, Lahlali T, Raab M, Michelet M, Romero-Lopez C, Rivoire M, et al. Reciprocal antagonism between the netrin-1 receptor uncoordinated-phenotype-5A (UNC5A) and the hepatitis C virus. Oncogene. 2017;36(48):6712-24. Epub 2017/08/08. doi: 10.1038/onc.2017.271. PubMed PMID: 28783179.
9. Plissonnier ML, Lahlali T, Michelet M, Lebosse F, Cottarel J, Beer M, et al. Epidermal Growth Factor Receptor-Dependent Mutual Amplification between Netrin-1 and the Hepatitis C Virus. PLoS Biol. 2016;14(3):e1002421. Epub 2016/04/01. doi: 10.1371/journal.pbio.1002421. PubMed PMID: 27031829.
10. Llambi F, Causeret F, Bloch-Gallego E, Mehlen P. Netrin-1 acts as a survival factor via its receptors UNC5H and DCC. The EMBO journal. 2001;20(11):2715-22. Epub 2001/06/02. doi: 10.1093/emboj/20.11.2715. PubMed PMID: 11387206; PubMed Central PMCID: PMC125255.
11. Thiebault K, Mazelin L, Pays L, Llambi F, Joly MO, Scoazec JY, et al. The netrin-1 receptors UNC5H are putative tumor suppressors controlling cell death commitment. Proceedings of the National Academy of Sciences of the United States of America. 2003;100(7):4173-8. Epub 2003/03/26. doi: 10.1073/pnas.0738063100. PubMed PMID: 12655055; PubMed Central PMCID: PMC153067.
12. Llambi F, Lourenco FC, Gozuacik D, Guix C, Pays L, Del Rio G, et al. The dependence receptor UNC5H2 mediates apoptosis through DAP-kinase. The EMBO

946 journal. 2005;24(6):1192-201. Epub 2005/02/25. doi: 10.1038/sj.emboj.7600584.
947 PubMed PMID: 15729359; PubMed Central PMCID: PMC556396.
948 13. Mille F, Llambi F, Guix C, Delloye-Bourgeois C, Guenebeaud C, Castro-
949 Obregon S, et al. Interfering with multimerization of netrin-1 receptors triggers tumor
950 cell death. Cell death and differentiation. 2009;16(10):1344-51. Epub 2009/06/23. doi:
951 10.1038/cdd.2009.75. PubMed PMID: 19543238; PubMed Central PMCID:
952 PMC2841642.
953 14. Guenebeaud C, Goldschneider D, Castets M, Guix C, Chazot G, Delloye-
954 Bourgeois C, et al. The dependence receptor UNC5H2/B triggers apoptosis via PP2A-
955 mediated dephosphorylation of DAP kinase. Molecular cell. 2010;40(6):863-76. Epub
956 2010/12/22. doi: 10.1016/j.molcel.2010.11.021. PubMed PMID: 21172653.
957 15. Paradisi A, Creveaux M, Gibert B, Devailly G, Redoulez E, Neves D, et al.
958 Combining chemotherapeutic agents and netrin-1 interference potentiates cancer cell
959 death. EMBO Mol Med. 2013;5(12):1821-34. Epub 2013/12/03. doi:
960 10.1002/emmm.201302654. PubMed PMID: 24293316.
961 16. Lahlali T, Plissonnier ML, Romero-Lopez C, Michelet M, Ducarouge B, Berzal-
962 Herranz A, et al. Netrin-1 Protects Hepatocytes Against Cell Death Through Sustained
963 Translation During the Unfolded Protein Response. Cell Mol Gastroenterol Hepatol.
964 2016;2(3):281-301 e9. Epub 2017/02/09. doi: 10.1016/j.jcmgh.2015.12.011. PubMed
965 PMID: 28174720; PubMed Central PMCID: PMCPMC5042567.
966 17. Asselah T, Bieche I, Mansouri A, Laurendeau I, Cazals-Hatem D, Feldmann G,
967 et al. In vivo hepatic endoplasmic reticulum stress in patients with chronic hepatitis C.
968 J Pathol. 2010;221(3):264-74. Epub 2010/06/09. doi: 10.1002/path.2703. PubMed
969 PMID: 20527020.
970 18. Joyce MA, Walters KA, Lamb SE, Yeh MM, Zhu LF, Kneteman N, et al. HCV
971 induces oxidative and ER stress, and sensitizes infected cells to apoptosis in
972 SCID/Alb-uPA mice. PLoS Pathog. 2009;5(2):e1000291. Epub 2009/02/27. doi:
973 10.1371/journal.ppat.1000291. PubMed PMID: 19242562; PubMed Central PMCID:
974 PMC2647842.
975 19. Maiers JL, Malhi H. Endoplasmic Reticulum Stress in Metabolic Liver Diseases
976 and Hepatic Fibrosis. Semin Liver Dis. 2019;39(2):235-48. Epub 2019/03/27. doi:
977 10.1055/s-0039-1681032. PubMed PMID: 30912096; PubMed Central PMCID:
978 PMCPMC6530577.
979 20. Hadi T, Boytard L, Silvestro M, Alebrahim D, Jacob S, Feinstein J, et al.
980 Macrophage-derived netrin-1 promotes abdominal aortic aneurysm formation by
981 activating MMP3 in vascular smooth muscle cells. Nat Commun. 2018;9(1):5022. Epub
982 2018/11/28. doi: 10.1038/s41467-018-07495-1. PubMed PMID: 30479344; PubMed
983 Central PMCID: PMCPMC6258757.
984 21. Mediero A, Wilder T, Ramkhelawon B, Moore KJ, Cronstein BN. Netrin-1 and
985 its receptor Unc5b are novel targets for the treatment of inflammatory arthritis. FASEB
986 J. 2016;30(11):3835-44. Epub 2016/11/03. doi: 10.1096/fj.201600615R. PubMed
987 PMID: 27502509; PubMed Central PMCID: PMCPMC5067256.
988 22. van Gils JM, Derby MC, Fernandes LR, Ramkhelawon B, Ray TD, Rayner KJ,
989 et al. The neuroimmune guidance cue netrin-1 promotes atherosclerosis by inhibiting
990 the emigration of macrophages from plaques. Nat Immunol. 2012;13(2):136-43. Epub
991 2012/01/11. doi: 10.1038/ni.2205. PubMed PMID: 22231519; PubMed Central PMCID:
992 PMC3262880.
993 23. Rosenberger P, Schwab JM, Mirakaj V, Masekowsky E, Mager A, Morote-
994 Garcia JC, et al. Hypoxia-inducible factor-dependent induction of netrin-1 dampens

995 inflammation caused by hypoxia. Nat Immunol. 2009;10(2):195-202. Epub 2009/01/06.
996 doi: 10.1038/ni.1683. PubMed PMID: 19122655.
997 24. Mirakaj V, Thix CA, Laucher S, Mielke C, Morote-Garcia JC, Schmit MA, et al.
998 Netrin-1 dampens pulmonary inflammation during acute lung injury. Am J Respir Crit
999 Care Med. 2010;181(8):815-24. Epub 2010/01/16. doi: 10.1164/rccm.200905-
1000 0717OC. PubMed PMID: 20075388.
1001 25. Aherne CM, Collins CB, Masterson JC, Tizzano M, Boyle TA, Westrich JA, et
1002 al. Neuronal guidance molecule netrin-1 attenuates inflammatory cell trafficking during
1003 acute experimental colitis. Gut. 2012;61(5):695-705. Epub 2011/08/05. doi:
1004 10.1136/gutjnl-2011-300012. PubMed PMID: 21813473; PubMed Central PMCID:
1005 PMC3322588.
1006 26. Paradisi A, Maisse C, Coissieux MM, Gadot N, Lepinasse F, Delloye-Bourgeois
1007 C, et al. Netrin-1 up-regulation in inflammatory bowel diseases is required for colorectal
1008 cancer progression. Proceedings of the National Academy of Sciences of the United
1009 States of America. 2009;106(40):17146-51. Epub 2009/09/02. doi:
1010 10.1073/pnas.0901767106. PubMed PMID: 19721007; PubMed Central PMCID:
1011 PMC2761333.
1012 27. Grandin M, Meier M, Delcros JG, Nikodemus D, Reuten R, Patel TR, et al.
1013 Structural Decoding of the Netrin-1/UNC5 Interaction and its Therapeutical
1014 Implications in Cancers. Cancer Cell. 2016;29(2):173-85. Epub 2016/02/10. doi:
1015 10.1016/j.ccell.2016.01.001. PubMed PMID: 26859457.
1016 28. Jungermann K, Kietzmann T. Zonation of parenchymal and nonparenchymal
1017 metabolism in liver. Annu Rev Nutr. 1996;16:179-203. Epub 1996/01/01. doi:
1018 10.1146/annurev.nu.16.070196.001143. PubMed PMID: 8839925.
1019 29. Lecluyse EL, Alexandre E. Isolation and culture of primary hepatocytes from
1020 resected human liver tissue. Methods Mol Biol. 2010;640:57-82. Epub 2010/07/21. doi:
1021 10.1007/978-1-60761-688-7_3. PubMed PMID: 20645046.
1022 30. Repetto G, del Peso A, Zurita JL. Neutral red uptake assay for the estimation of
1023 cell viability/cytotoxicity. Nat Protoc. 2008;3(7):1125-31. Epub 2008/07/05. doi:
1024 10.1038/nprot.2008.75. PubMed PMID: 18600217.
1025 31. Parent R, Kolippakkam D, Booth G, Beretta L. Mammalian target of rapamycin
1026 activation impairs hepatocytic differentiation and targets genes moderating lipid
1027 homeostasis and hepatocellular growth. Cancer research. 2007;67(9):4337-45. Epub
1028 2007/05/08. doi: 10.1158/0008-5472.can-06-3640. PubMed PMID: 17483347.
1029 32. Stephens SB, Nicchitta CV. In vitro and tissue culture methods for analysis of
1030 translation initiation on the endoplasmic reticulum. Methods Enzymol. 2007;431:47-60.
1031 Epub 2007/10/10. doi: 10.1016/S0076-6879(07)31004-5. PubMed PMID: 17923230.
1032 33. Stephens SB, Dodd RD, Lerner RS, Pyhtila BM, Nicchitta CV. Analysis of mRNA
1033 partitioning between the cytosol and endoplasmic reticulum compartments of
1034 mammalian cells. Methods Mol Biol. 2008;419:197-214. Epub 2008/03/29. doi:
1035 10.1007/978-1-59745-033-1_14. PubMed PMID: 18369985.
1036 34. Casabona MG, Vandenbrouck Y, Attree I, Coute Y. Proteomic characterization
1037 of Pseudomonas aeruginosa PAO1 inner membrane. Proteomics. 2013;13(16):2419-
1038 23. Epub 2013/06/08. doi: 10.1002/pmic.201200565. PubMed PMID: 23744604.
1039 35. Tyanova S, Temu T, Cox J. The MaxQuant computational platform for mass
1040 spectrometry-based shotgun proteomics. Nat Protoc. 2016;11(12):2301-19. Epub
1041 2016/11/04. doi: 10.1038/nprot.2016.136. PubMed PMID: 27809316.
1042 36. Boncompain G, Perez F. Fluorescence-based analysis of trafficking in
1043 mammalian cells. Methods Cell Biol. 2013;118:179-94. Epub 2013/12/04. doi:
1044 10.1016/B978-0-12-417164-0.00011-2. PubMed PMID: 24295307.

37. Sanjana NE, Shalem O, Zhang F. Improved vectors and genome-wide libraries for CRISPR screening. Nat Methods. 2014;11(8):783-4. Epub 2014/07/31. doi: 10.1038/nmeth.3047. PubMed PMID: 25075903; PubMed Central PMCID: PMCPMC4486245.
38. Bassot A, Chauvin MA, Bendridi N, Ji-Cao J, Vial G, Monnier L, et al. Regulation of Mitochondria-Associated Membranes (MAMs) by NO/sGC/PKG Participates in the Control of Hepatic Insulin Response. Cells. 2019;8(11). Epub 2019/11/17. doi: 10.3390/cells8111319. PubMed PMID: 31731523; PubMed Central PMCID: PMCPMC6912364.
39. Friedman SL. Hepatic stellate cells: protean, multifunctional, and enigmatic cells of the liver. Physiol Rev. 2008;88(1):125-72. Epub 2008/01/16. doi: 10.1152/physrev.00013.2007. PubMed PMID: 18195085; PubMed Central PMCID: PMCPMC2888531.
40. Koyama Y, Brenner DA. Liver inflammation and fibrosis. J Clin Invest. 2017;127(1):55-64. Epub 2017/01/04. doi: 10.1172/JCI88881. PubMed PMID: 28045404; PubMed Central PMCID: PMCPMC5199698.
41. Parent R, Marion MJ, Furio L, Trepo C, Petit MA. Origin and characterization of a human bipotent liver progenitor cell line. Gastroenterology. 2004;126(4):1147-56. Epub 2004/04/02. PubMed PMID: 15057753.
42. Gripon P, Rumin S, Urban S, Le Seyec J, Glaise D, Cannie I, et al. Infection of a human hepatoma cell line by hepatitis B virus. Proceedings of the National Academy of Sciences of the United States of America. 2002;99(24):15655-60. Epub 2002/11/15. doi: 10.1073/pnas.232137699. PubMed PMID: 12432097; PubMed Central PMCID: PMC137772.
43. Saito T, Owen DM, Jiang F, Marcotrigiano J, Gale M, Jr. Innate immunity induced by composition-dependent RIG-I recognition of hepatitis C virus RNA. Nature. 2008;454(7203):523-7. Epub 2008/06/13. doi: 10.1038/nature07106. PubMed PMID: 18548002; PubMed Central PMCID: PMCPMC2856441.
44. Sato S, Li K, Kameyama T, Hayashi T, Ishida Y, Murakami S, et al. The RNA sensor RIG-I dually functions as an innate sensor and direct antiviral factor for hepatitis B virus. Immunity. 2015;42(1):123-32. Epub 2015/01/06. doi: 10.1016/j.immuni.2014.12.016. PubMed PMID: 25557055.
45. Maire M, Parent R, Morand AL, Alotte C, Trepo C, Durantel D, et al. Characterization of the double-stranded RNA responses in human liver progenitor cells. Biochemical and biophysical research communications. 2008;368(3):556-62. Epub 2008/02/09. doi: 10.1016/j.bbrc.2008.01.123. PubMed PMID: 18258184.
46. Leclere L, Rentzsch F. Repeated evolution of identical domain architecture in metazoan netrin domain-containing proteins. Genome Biol Evol. 2012;4(9):883-99. Epub 2012/07/21. doi: 10.1093/gbe/evs061. PubMed PMID: 22813778; PubMed Central PMCID: PMCPMC3516229.
47. Vispe S, DeVries L, Creancier L, Besse J, Breand S, Hobson DJ, et al. Triptolide is an inhibitor of RNA polymerase I and II-dependent transcription leading predominantly to down-regulation of short-lived mRNA. Mol Cancer Ther. 2009;8(10):2780-90. Epub 2009/10/08. doi: 10.1158/1535-7163.MCT-09-0549. PubMed PMID: 19808979.
48. Barnault R, Lahlali T, Plissonnier ML, Romero-Lopez C, Laverdure N, Ducarouge B, et al. Hepatocellular carcinoma-associated depletion of the netrin-1 receptor Uncoordinated Phenotype-5A (UNC5A) skews the hepatic unfolded protein response towards prosurvival outcomes. Biochem Biophys Res Commun.

2018;495(4):2425-31. Epub 2017/12/27. doi: 10.1016/j.bbrc.2017.12.129. PubMed PMID: 29277614.
49. Reid DW, Nicchitta CV. Primary role for endoplasmic reticulum-bound ribosomes in cellular translation identified by ribosome profiling. J Biol Chem. 2012;287(8):5518-27. Epub 2011/12/27. doi: 10.1074/jbc.M111.312280. PubMed PMID: 22199352; PubMed Central PMCID: PMCPMC3285328.
50. Chen Q, Jagannathan S, Reid DW, Zheng T, Nicchitta CV. Hierarchical regulation of mRNA partitioning between the cytoplasm and the endoplasmic reticulum of mammalian cells. Mol Biol Cell. 2011;22(14):2646-58. Epub 2011/05/27. doi: 10.1091/mbc.E11-03-0239. PubMed PMID: 21613539; PubMed Central PMCID: PMCPMC3135488.
51. Wickham L, Duchaine T, Luo M, Nabi IR, DesGroseillers L. Mammalian staufen is a double-stranded-RNA- and tubulin-binding protein which localizes to the rough endoplasmic reticulum. Mol Cell Biol. 1999;19(3):2220-30. Epub 1999/02/18. doi: 10.1128/mcb.19.3.2220. PubMed PMID: 10022909; PubMed Central PMCID: PMCPMC84015.
52. Marion RM, Fortes P, Beloso A, Dotti C, Ortin J. A human sequence homologue of Staufen is an RNA-binding protein that is associated with polysomes and localizes to the rough endoplasmic reticulum. Mol Cell Biol. 1999;19(3):2212-9. Epub 1999/02/18. doi: 10.1128/mcb.19.3.2212. PubMed PMID: 10022908; PubMed Central PMCID: PMCPMC84014.
53. Dugre-Brisson S, Elvira G, Boulay K, Chatel-Chaix L, Mouland AJ, DesGroseillers L. Interaction of Staufen1 with the 5' end of mRNA facilitates translation of these RNAs. Nucleic Acids Res. 2005;33(15):4797-812. Epub 2005/08/30. doi: 10.1093/nar/gki794. PubMed PMID: 16126845; PubMed Central PMCID: PMCPMC1193567.
54. Ricci EP, Kucukural A, Cenik C, Mercier BC, Singh G, Heyer EE, et al. Staufen1 senses overall transcript secondary structure to regulate translation. Nat Struct Mol Biol. 2014;21(1):26-35. Epub 2013/12/18. doi: 10.1038/nsmb.2739. PubMed PMID: 24336223; PubMed Central PMCID: PMCPMC4605437.
55. Furic L, Maher-Laporte M, DesGroseillers L. A genome-wide approach identifies distinct but overlapping subsets of cellular mRNAs associated with Staufen1- and Staufen2-containing ribonucleoprotein complexes. RNA. 2008;14(2):324-35. Epub 2007/12/21. doi: 10.1261/rna.720308. PubMed PMID: 18094122; PubMed Central PMCID: PMCPMC2212254.
56. de Lucas S, Oliveros JC, Chagoyen M, Ortin J. Functional signature for the recognition of specific target mRNAs by human Staufen1 protein. Nucleic Acids Res. 2014;42(7):4516-26. Epub 2014/01/29. doi: 10.1093/nar/gku073. PubMed PMID: 24470147; PubMed Central PMCID: PMCPMC3985646.
57. Villace P, Marion RM, Ortin J. The composition of Staufen-containing RNA granules from human cells indicates their role in the regulated transport and translation of messenger RNAs. Nucleic Acids Res. 2004;32(8):2411-20. Epub 2004/05/04. doi: 10.1093/nar/gkh552. PubMed PMID: 15121898; PubMed Central PMCID: PMCPMC419443.
58. Kohrmann M, Luo M, Kaether C, DesGroseillers L, Dotti CG, Kiebler MA. Microtubule-dependent recruitment of Staufen-green fluorescent protein into large RNA-containing granules and subsequent dendritic transport in living hippocampal neurons. Mol Biol Cell. 1999;10(9):2945-53. Epub 1999/09/03. doi: 10.1091/mbc.10.9.2945. PubMed PMID: 10473638; PubMed Central PMCID: PMCPMC25535.

59. Fang J, Pietzsch C, Ramanathan P, Santos RI, Ilinykh PA, Garcia-Blanco MA, et al. Staufen1 Interacts with Multiple Components of the Ebola Virus Ribonucleoprotein and Enhances Viral RNA Synthesis. mBio. 2018;9(5). Epub 2018/10/12. doi: 10.1128/mBio.01771-18. PubMed PMID: 30301857; PubMed Central PMCID: PMCPMC6178623.
60. Taketa K, Pogell BM. Allosteric Inhibition of Rat Liver Fructose 1,6-Diphosphatase by Adenosine 5'-Monophosphate. J Biol Chem. 1965;240:651-62. Epub 1965/02/01. PubMed PMID: 14275118.
61. Schlegel M, Kohler D, Korner A, Granja T, Straub A, Giera M, et al. The neuroimmune guidance cue netrin-1 controls resolution programs and promotes liver regeneration. Hepatology. 2015. Epub 2015/11/18. doi: 10.1002/hep.28347. PubMed PMID: 26573873.
62. El-Serag HB, Marrero JA, Rudolph L, Reddy KR. Diagnosis and treatment of hepatocellular carcinoma. Gastroenterology. 2008;134(6):1752-63. Epub 2008/05/13. doi: 10.1053/j.gastro.2008.02.090
S0016-5085(08)00426-5 [pii]. PubMed PMID: 18471552.
63. Umemura A, Park EJ, Taniguchi K, Lee JH, Shalapour S, Valasek MA, et al. Liver damage, inflammation, and enhanced tumorigenesis after persistent mTORC1 inhibition. Cell Metab. 2014;20(1):133-44. Epub 2014/06/10. doi: 10.1016/j.cmet.2014.05.001. PubMed PMID: 24910242; PubMed Central PMCID: PMCPMC4079758.
64. He G, Dhar D, Nakagawa H, Font-Burgada J, Ogata H, Jiang Y, et al. Identification of liver cancer progenitors whose malignant progression depends on autocrine IL-6 signaling. Cell. 2013;155(2):384-96. Epub 2013/10/15. doi: 10.1016/j.cell.2013.09.031. PubMed PMID: 24120137; PubMed Central PMCID: PMCPMC4015514.
65. Park EJ, Lee JH, Yu GY, He G, Ali SR, Holzer RG, et al. Dietary and genetic obesity promote liver inflammation and tumorigenesis by enhancing IL-6 and TNF expression. Cell. 2010;140(2):197-208. Epub 2010/02/10. doi: 10.1016/j.cell.2009.12.052. PubMed PMID: 20141834; PubMed Central PMCID: PMCPMC2836922.
66. Naugler WE, Sakurai T, Kim S, Maeda S, Kim K, Elsharkawy AM, et al. Gender disparity in liver cancer due to sex differences in MyD88-dependent IL-6 production. Science. 2007;317(5834):121-4. Epub 2007/07/07. doi: 10.1126/science.1140485. PubMed PMID: 17615358.
67. Odom DT, Zizlsperger N, Gordon DB, Bell GW, Rinaldi NJ, Murray HL, et al. Control of pancreas and liver gene expression by HNF transcription factors. Science. 2004;303(5662):1378-81. Epub 2004/02/28. doi: 10.1126/science.1089769. PubMed PMID: 14988562; PubMed Central PMCID: PMCPMC3012624.
68. Knight JRP, Alexandrou C, Skalka GL, Vlahov N, Pennel K, Officer L, et al. MNK inhibition sensitizes KRAS-mutant colorectal cancer to mTORC1 inhibition by reducing eIF4E phosphorylation and c-MYC expression. Cancer Discov. 2020. Epub 2020/12/18. doi: 10.1158/2159-8290.CD-20-0652. PubMed PMID: 33328217.
69. Boussemart L, Malka-Mahieu H, Girault I, Allard D, Hemmingsson O, Tomasic G, et al. eIF4F is a nexus of resistance to anti-BRAF and anti-MEK cancer therapies. Nature. 2014;513(7516):105-9. Epub 2014/08/01. doi: 10.1038/nature13572. PubMed PMID: 25079330.
70. Parent R, Beretta L. Translational control plays a prominent role in the hepatocytic differentiation of HepaRG liver progenitor cells. Genome Biol.

2008;9(1):R19. Epub 2008/01/29. doi: 10.1186/gb-2008-9-1-r19. PubMed PMID: 18221535; PubMed Central PMCID: PMC2395229.
71. Sahin F, Kannangai R, Adegbola O, Wang J, Su G, Torbenson M. mTOR and P70 S6 kinase expression in primary liver neoplasms. Clin Cancer Res. 2004;10(24):8421-5. Epub 2004/12/30. doi: 10.1158/1078-0432.CCR-04-0941. PubMed PMID: 15623621.
72. Lahlali T, Plissonnier ML, Romero-López C, Michelet M, Ducarouge B, Berzal-Herranz A, et al. Netrin-1 Protects Hepatocytes Against Cell Death Through Sustained Translation During the Unfolded Protein Response. Cell Mol Gastroenterol Hepatol. 2016;2(3):281-301.e9. Epub 2017/02/09. doi: 10.1016/j.jcmgh.2015.12.011. PubMed PMID: 28174720; PubMed Central PMCID: PMCPMC5042567.
73. Xu TP, Wang YF, Xiong WL, Ma P, Wang WY, Chen WM, et al. E2F1 induces TINCR transcriptional activity and accelerates gastric cancer progression via activation of TINCR/STAU1/CDKN2B signaling axis. Cell Death Dis. 2017;8(6):e2837. Epub 2017/06/02. doi: 10.1038/cddis.2017.205. PubMed PMID: 28569791; PubMed Central PMCID: PMCPMC5520882.
74. Xu F, Li CH, Wong CH, Chen GG, Lai PBS, Shao S, et al. Genome-Wide Screening and Functional Analysis Identifies Tumor Suppressor Long Noncoding RNAs Epigenetically Silenced in Hepatocellular Carcinoma. Cancer Res. 2019;79(7):1305-17. Epub 2019/02/06. doi: 10.1158/0008-5472.CAN-18-1659. PubMed PMID: 30718359.
75. He G, Karin M. NF-kappaB and STAT3 - key players in liver inflammation and cancer. Cell Res. 2011;21(1):159-68. Epub 2010/12/29. doi: 10.1038/cr.2010.183. PubMed PMID: 21187858; PubMed Central PMCID: PMCPMC3193410.
76. Mehlen P, Delloye-Bourgeois C, Chedotal A. Novel roles for Slits and netrins: axon guidance cues as anticancer targets? Nature reviews Cancer. 2011;11(3):188-97. Epub 2011/02/18. doi: 10.1038/nrc3005. PubMed PMID: 21326323.
77. Gao R, Peng X, Perry C, Sun H, Ntokou A, Ryu C, et al. Macrophage-derived netrin-1 drives adrenergic nerve-associated lung fibrosis. J Clin Invest. 2021;131(1). Epub 2021/01/05. doi: 10.1172/JCI136542. PubMed PMID: 33393489; PubMed Central PMCID: PMCPMC7773383.
78. Romanowski T, Sikorska K, Bielawski KP. GUS and PMM1 as suitable reference genes for gene expression analysis in the liver tissue of patients with chronic hepatitis. Med Sci Monit. 2008;14(7):BR147-52. Epub 2008/07/02. PubMed PMID: 18591914.

Figure 1

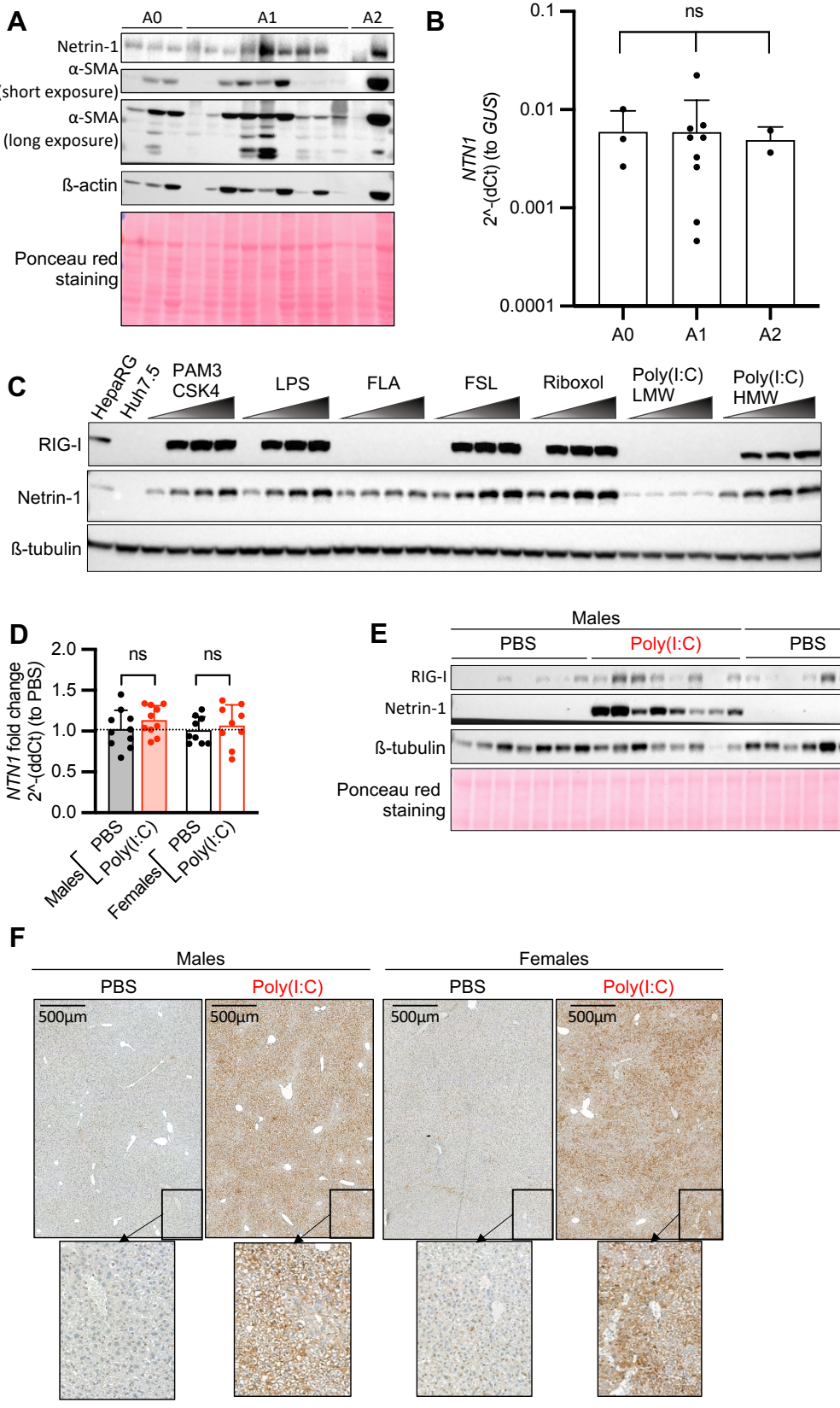
A
A0
A1
A2
Netrin-1
α-SMA
(short exposure)
α-SMA
(long exposure)
ß-actin
Ponceau red
staining
B
ns
0.1
0.01
0.001
0.0001
NTN1
2^-(dCt) (to GUS)
A0
A1
A2
C
HepaRG
Huh7.5
PAM3
CSK4
LPS
FLA
FSL
Riboxol
Poly(I:C)
LMW
Poly(I:C)
HMW
RIG-I
Netrin-1
ß-tubulin
D
ns
ns
2.0
1.5
1.0
0.5
0.0
NTN1 fold change
2^-(ddCt) (to PBS)
PBS
Poly(I:C)
PBS
Poly(I:C)
Males
Females
E
Males
Females
PBS
Poly(I:C)
PBS
Poly(I:C)
RIG-I
Netrin-1
ß-tubulin
Ponceau red
staining
F
Males
Females
PBS
Poly(I:C)
PBS
Poly(I:C)
500µm
500µm
500µm
500µm

Figure 2

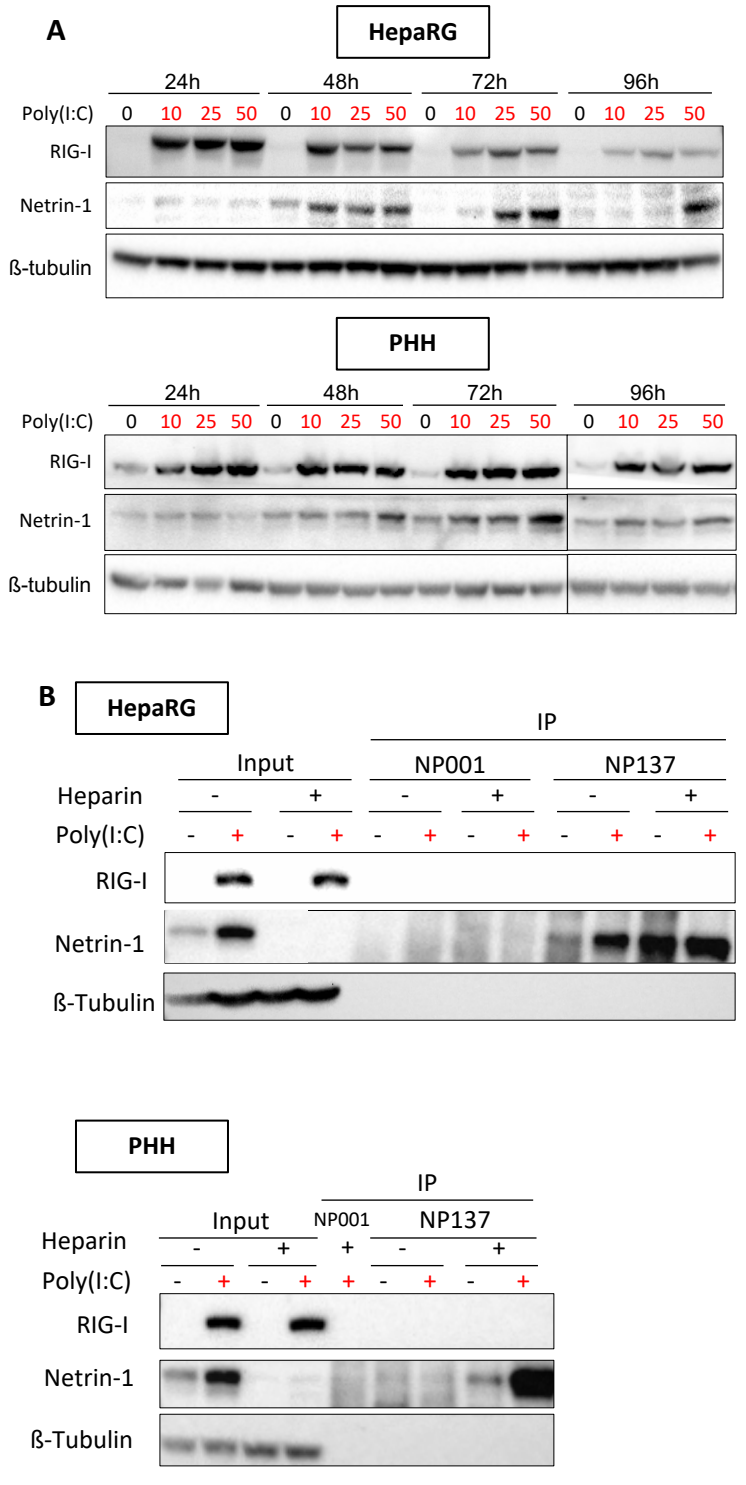
A
HepaRG
24h
48h
72h
96h
Poly(I:C)
0 10 25 50 0 10 25 50 0 10 25 50 0 10 25 50
RIG-I
Netrin-1
ß-tubulin
PHH
24h
48h
72h
96h
Poly(I:C)
0 10 25 50 0 10 25 50 0 10 25 50 0 10 25 50
RIG-I
Netrin-1
ß-tubulin
B
HepaRG
IP
Input
NP001
NP137
Heparin
- + - + - +
Poly(I:C)
- + - + - + - + - + - +
RIG-I
Netrin-1
ß-Tubulin
PHH
IP
Input
NP001
NP137
Heparin
- + + - +
Poly(I:C)
- + - + + - + - +
RIG-I
Netrin-1
ß-Tubulin

Figure 3

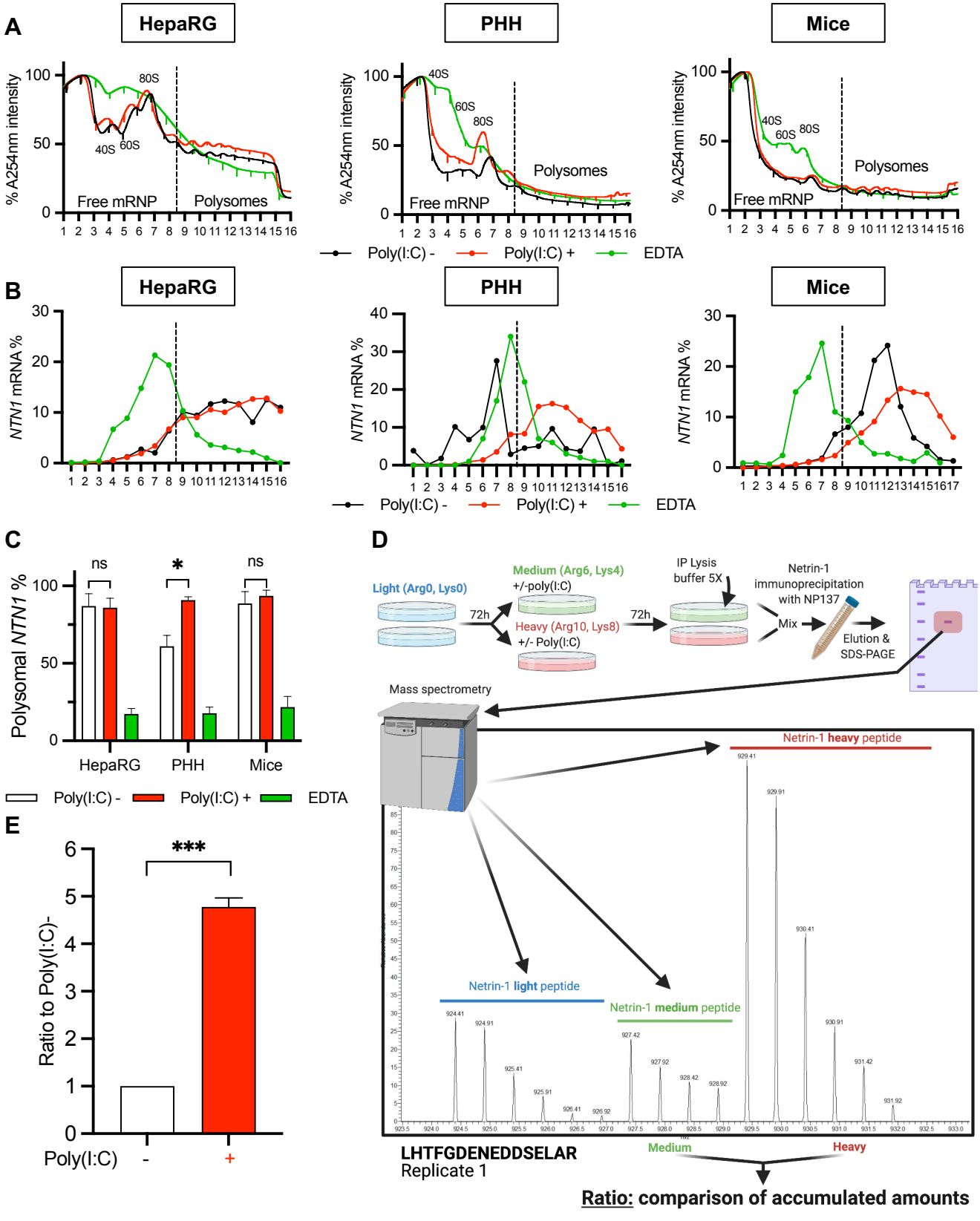
A
HepaRG
PHH
Mice
% A254nm intensity
40S
60S
80S
Free mRNP
Polysomes
Poly(I:C) -
Poly(I:C) +
EDTA
B
NTN1 mRNA %
C
Polysomal NTN1 %
ns
*
ns
HepaRG
PHH
Mice
D
Light (Arg0, Lys0)
Medium (Arg6, Lys4)
+/-poly(I:C)
Heavy (Arg10, Lys8)
+/- Poly(I:C)
72h
IP Lysis buffer 5X
Netrin-1 immunoprecipitation with NP137
Mix
Elution & SDS-PAGE
Mass spectrometry
Netrin-1 heavy peptide
Netrin-1 light peptide
Netrin-1 medium peptide
LHTFGDENEDDSELAR
Replicate 1
Medium
Heavy
Ratio: comparison of accumulated amounts
E
***
Ratio to Poly(I:C)-
Poly(I:C)

Figure 4

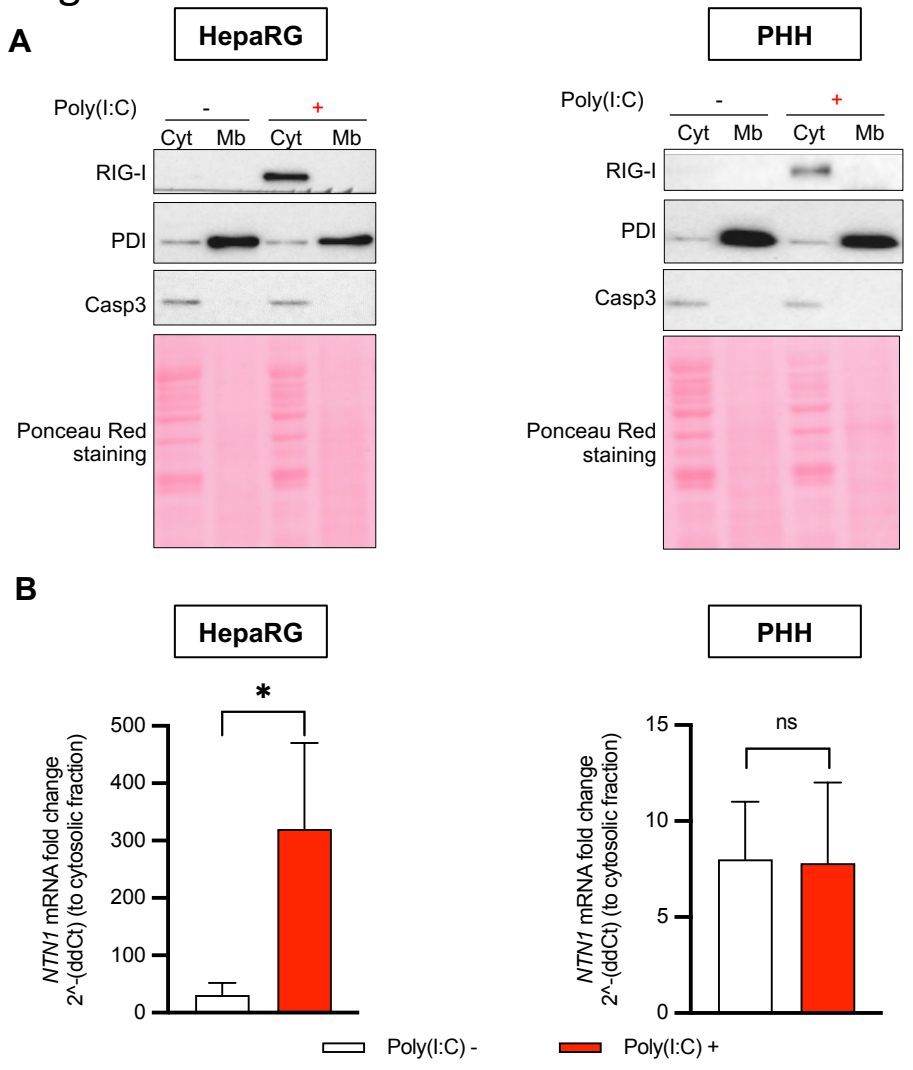
A
HepaRG
PHH
Poly(I:C)
-
+
Cyt
Mb
RIG-I
PDI
Casp3
Ponceau Red staining
B
HepaRG
PHH
*
ns
NTN1 mRNA fold change 2^-(ddCt) (to cytosolic fraction)
500
400
300
200
100
0
15
10
5
Poly(I:C) -
Poly(I:C) +

Figure 5

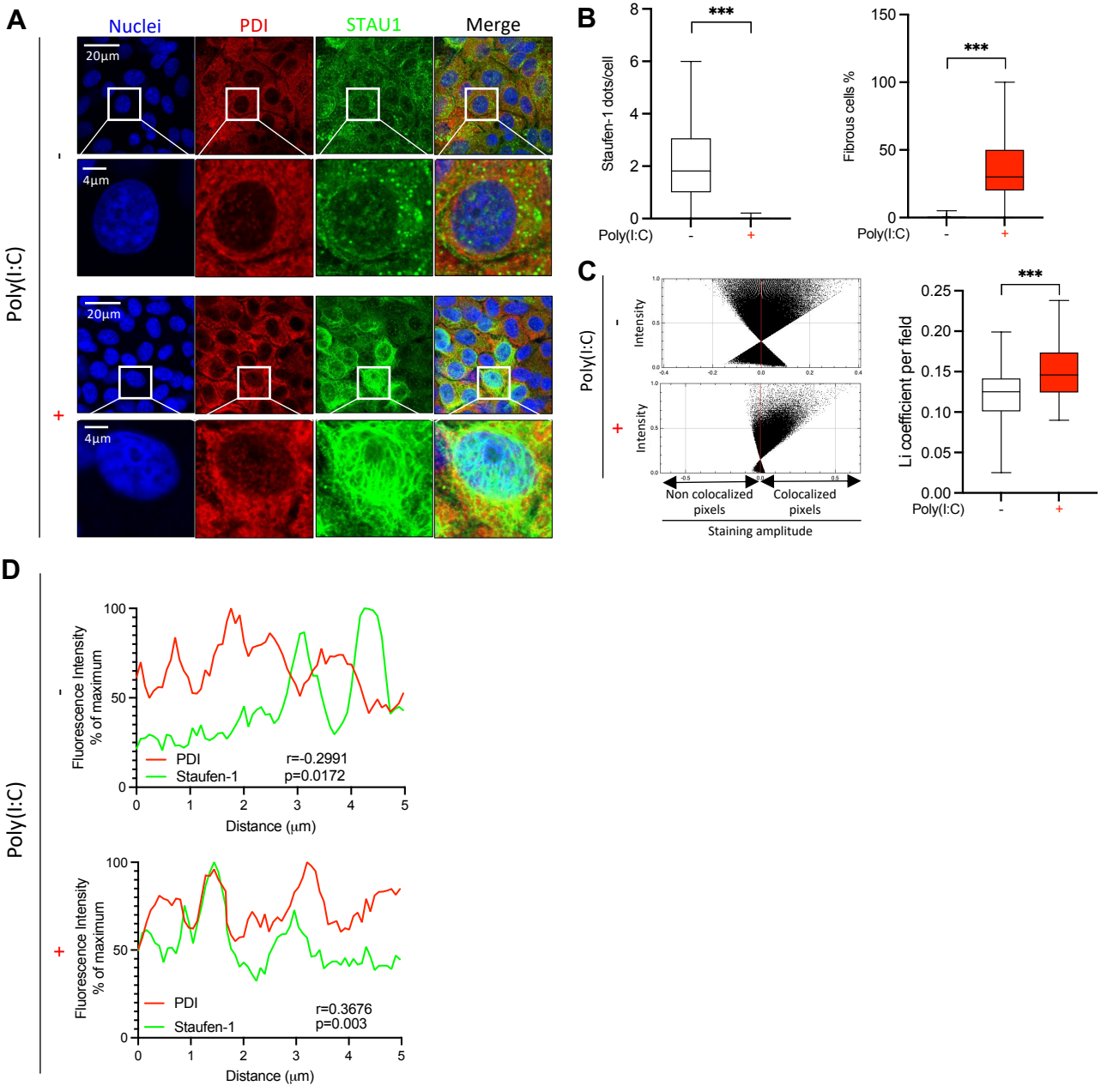
A
Nuclei
PDI
STAU1
Merge
20µm
4µm
Poly(I:C)
-
+
B
Staufen-1 dots/cell
***
Poly(I:C)
Fibrous cells %
C
Intensity
Non colocalized pixels
Colocalized pixels
Staining amplitude
Li coefficient per field
D
Fluorescence Intensity % of maximum
PDI
Staufen-1
r=-0.2991
p=0.0172
Distance (µm)
r=0.3676
p=0.003

Figure 6

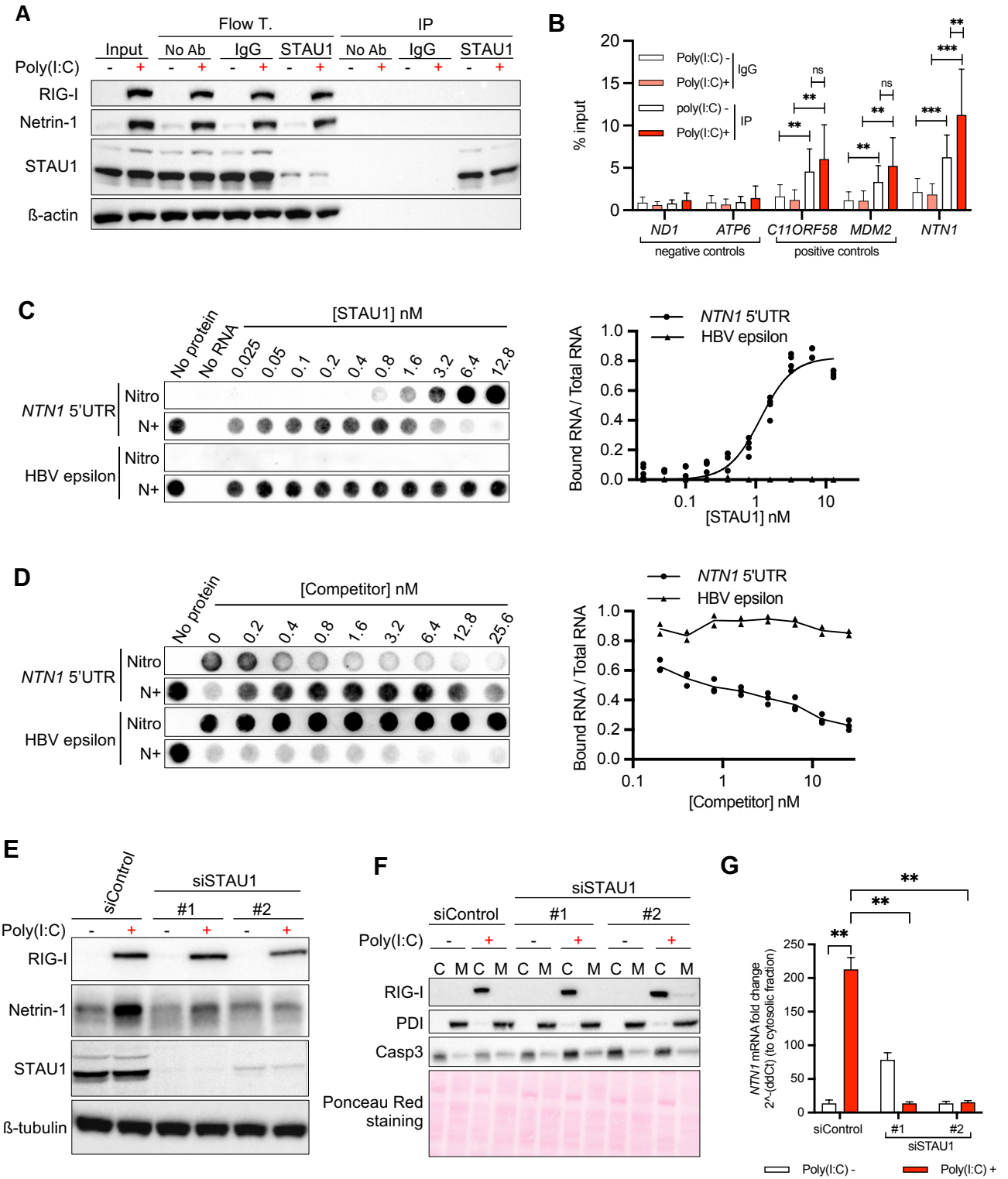
A
Flow T.
IP
Input
No Ab
IgG
STAU1
No Ab
IgG
STAU1
Poly(I:C)
- + - + - + - + - + - + - +
RIG-I
Netrin-1
STAU1
ß-actin
B
% input
Poly(I:C) -
Poly(I:C)+
IgG
poly(I:C) -
Poly(I:C)+
IP
ns
**
***
ND1
ATP6
C11ORF58
MDM2
NTN1
negative controls
positive controls
C
No protein
No RNA
[STAU1] nM
0.025
0.05
0.1
0.2
0.4
0.8
1.6
3.2
6.4
12.8
NTN1 5'UTR
Nitro
N+
HBV epsilon
Nitro
N+
NTN1 5'UTR
HBV epsilon
Bound RNA / Total RNA
[STAU1] nM
D
No protein
[Competitor] nM
0
0.2
0.4
0.8
1.6
3.2
6.4
12.8
25.6
NTN1 5'UTR
Nitro
N+
HBV epsilon
Nitro
N+
NTN1 5'UTR
HBV epsilon
Bound RNA / Total RNA
[Competitor] nM
E
siControl
siSTAU1
#1
#2
Poly(I:C)
- + - + - +
RIG-I
Netrin-1
STAU1
ß-tubulin
F
siSTAU1
siControl
#1
#2
Poly(I:C)
- + - + - +
C M C M C M C M C M C M
RIG-I
PDI
Casp3
Ponceau Red staining
G
NTN1 mRNA fold change 2^-(ddCt) (to cytosolic fraction)
siControl
#1
#2
siSTAU1
Poly(I:C) -
Poly(I:C) +

Figure 7

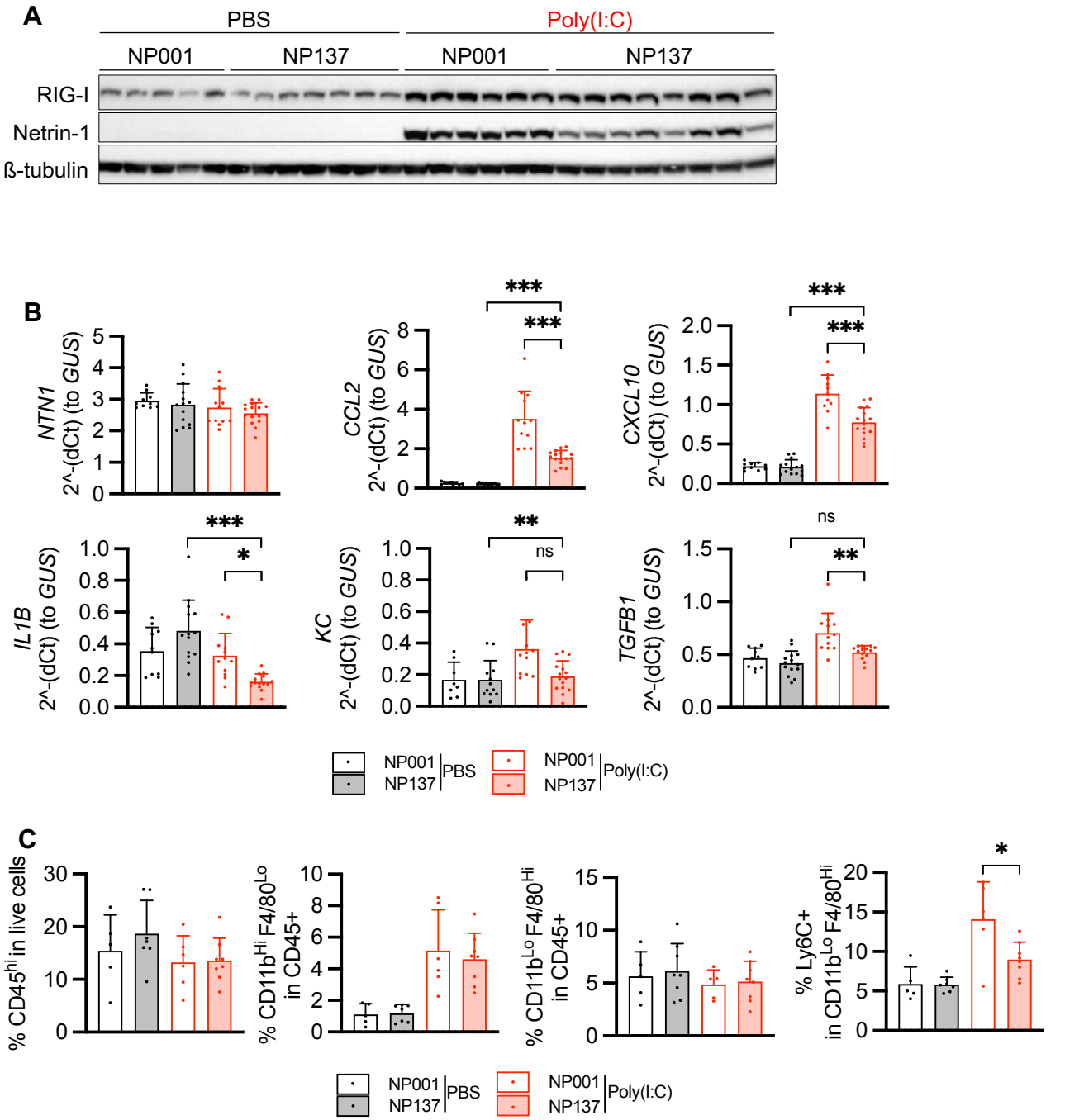
A
PBS
Poly(I:C)
NP001
NP137
NP001
NP137
RIG-I
Netrin-1
ß-tubulin
B
NTN1
2^-(dCt) (to GUS)
CCL2
CXCL10
IL1B
KC
TGFB1
***
**
*
ns
NP001
NP137
PBS
Poly(I:C)
C
% CD45hi in live cells
% CD11bHi F4/80Lo in CD45+
% CD11bLo F4/80Hi in CD45+
% Ly6C+ in CD11bLo F4/80Hi

Figure 8

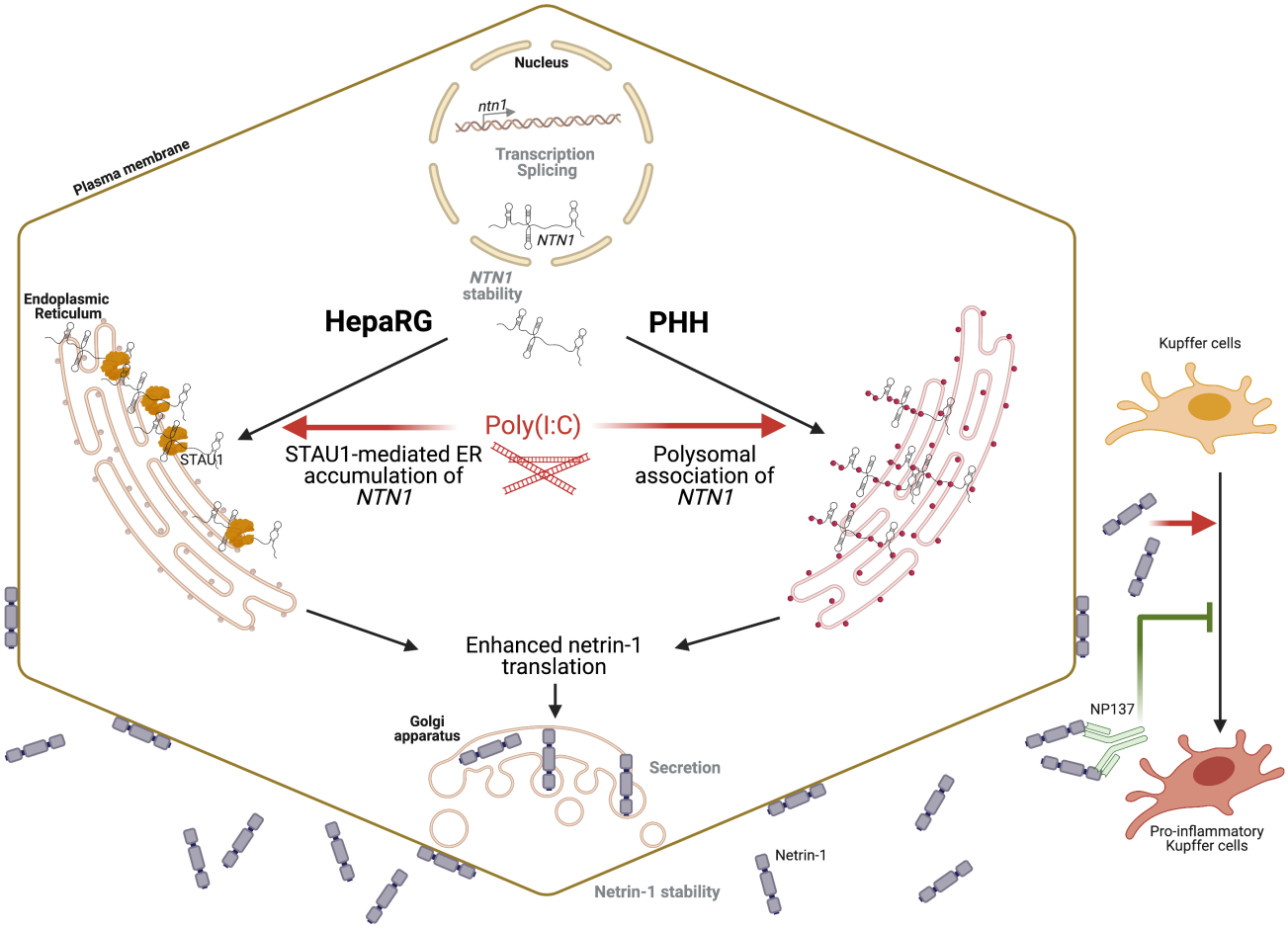
Plasma membrane
Nucleus
ntn1
Transcription
Splicing
NTN1
NTN1
stability
Endoplasmic
Reticulum
HepaRG
PHH
STAU1
Poly(I:C)
STAU1-mediated ER
accumulation of
NTN1
Polysomal
association of
NTN1
Kupffer cells
Enhanced netrin-1
translation
Golgi
apparatus
Secretion
NP137
Pro-inflammatory
Kupffer cells
Netrin-1
Netrin-1 stability

Supplementary figure 1

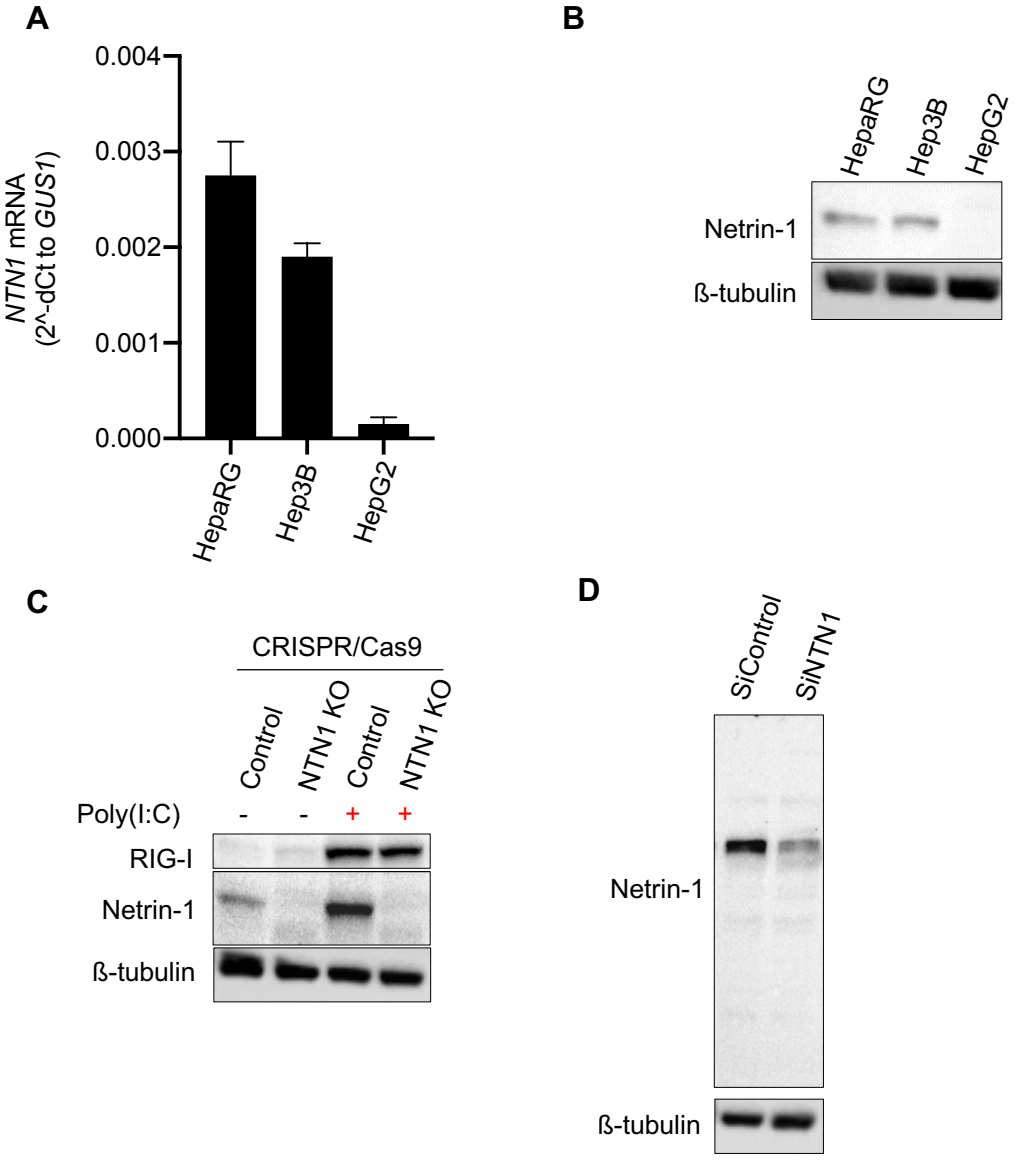

Supplementary figure 2

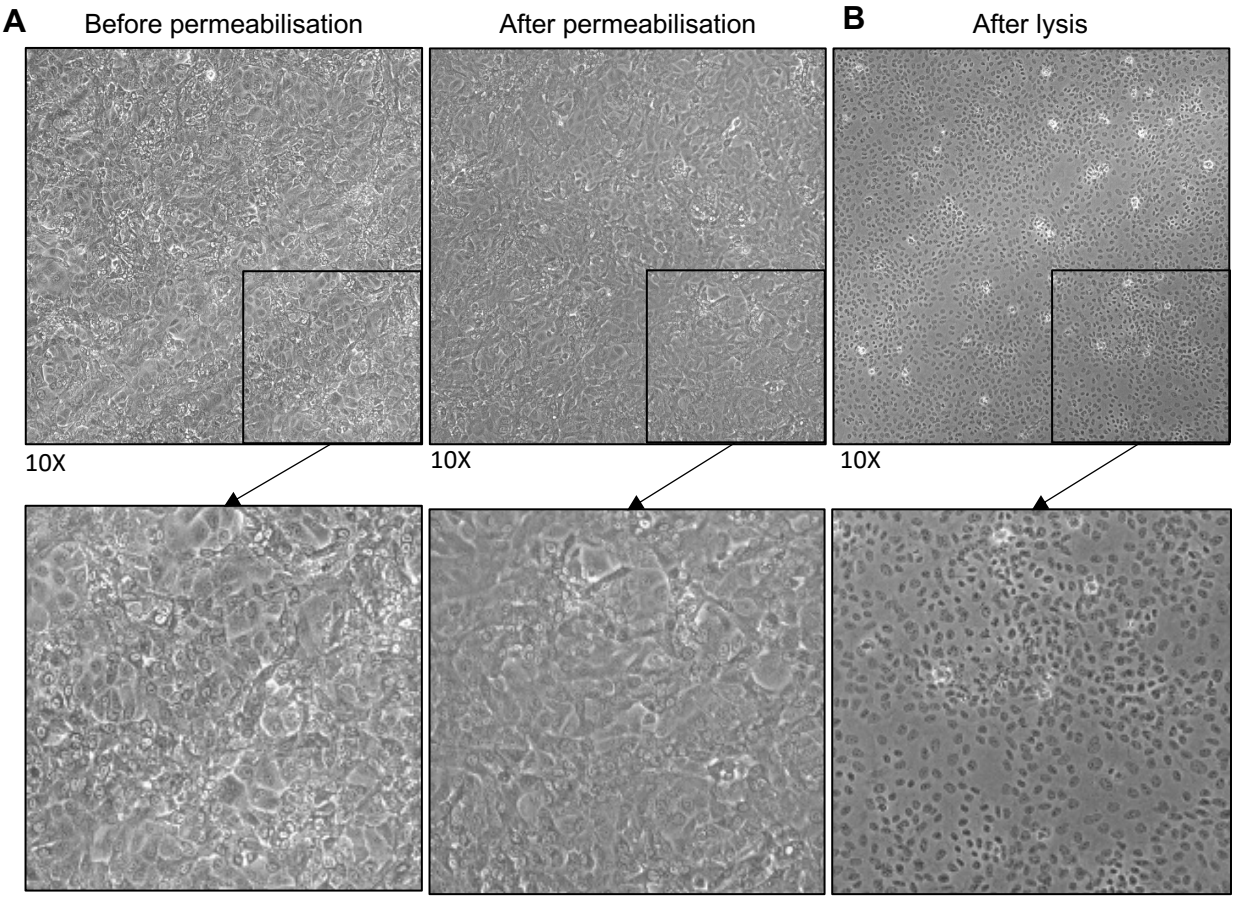

Supplementary figure 3

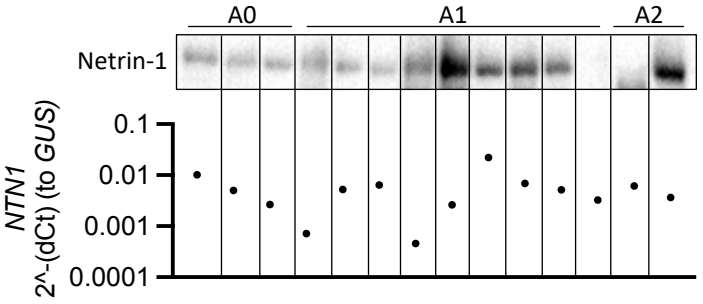

Supplementary figure 4

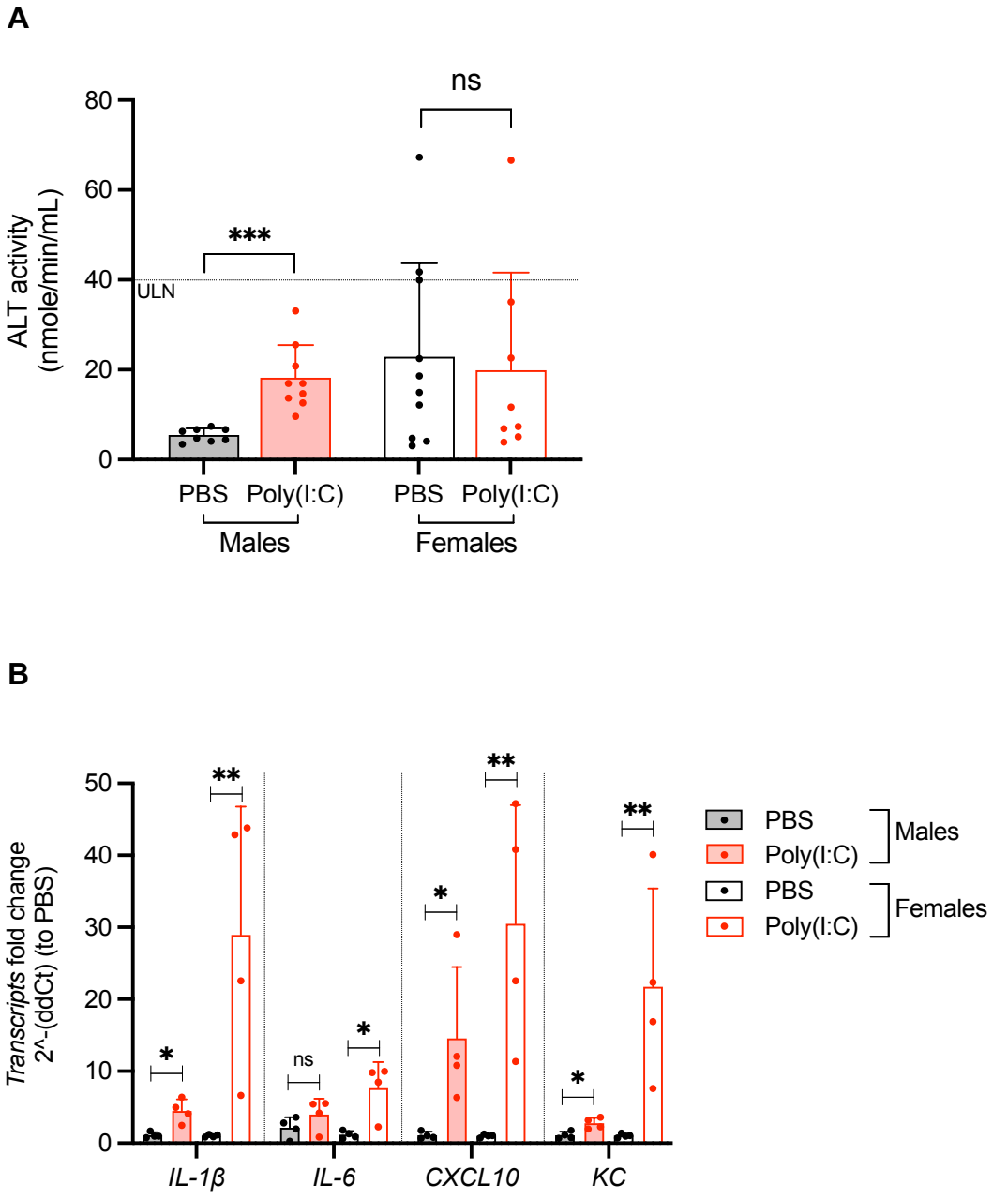

Supplementary figure 5

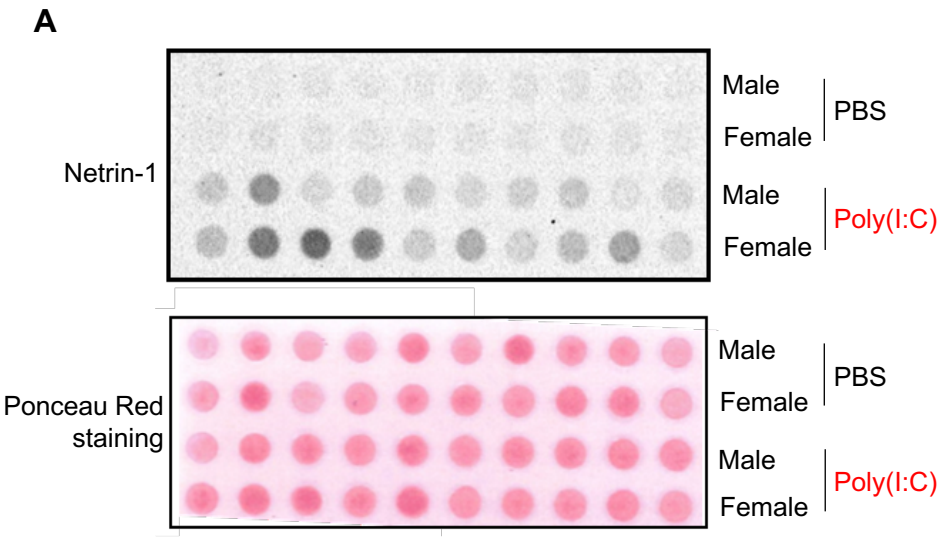

Supplementary figure 6

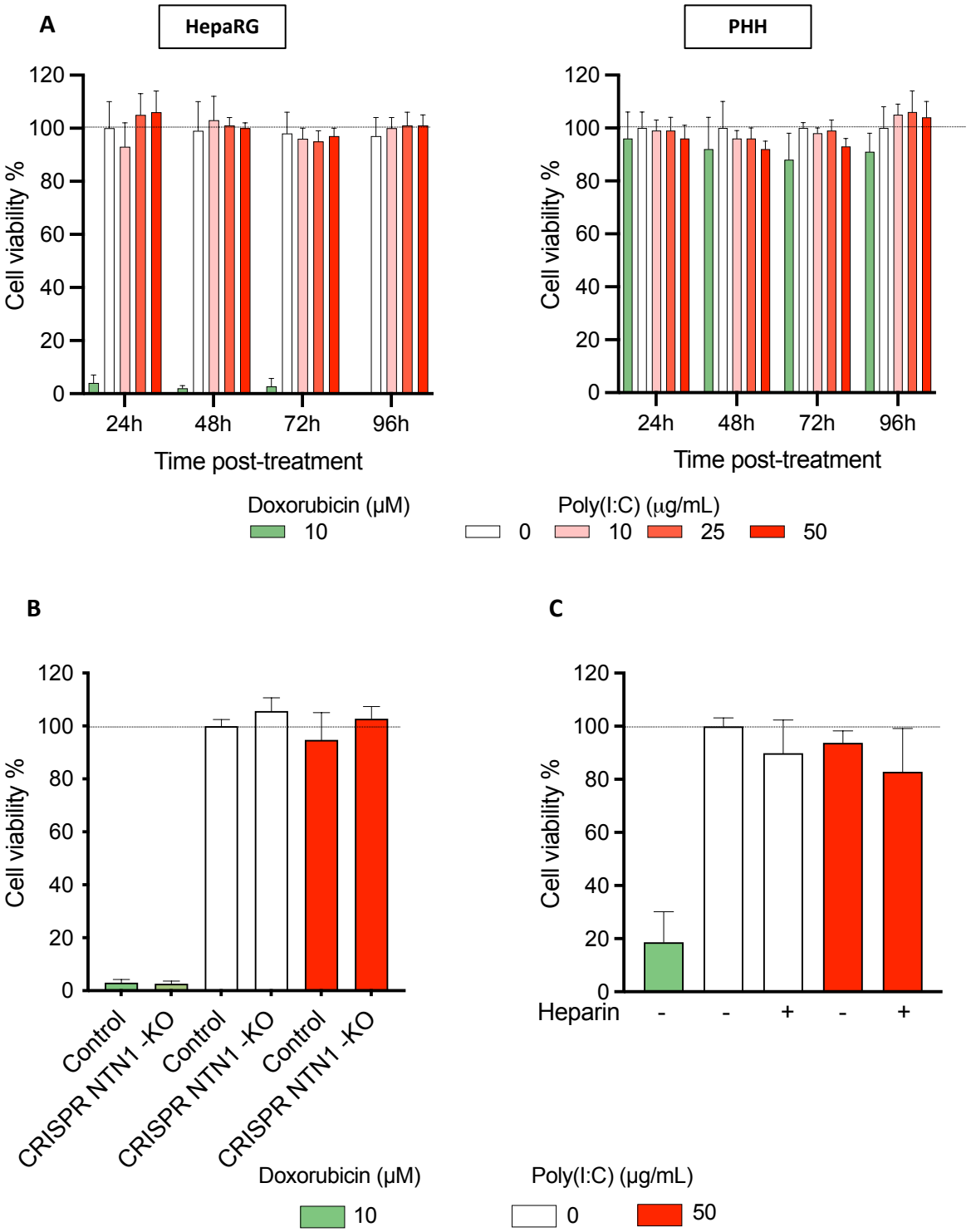

Supplementary figure 7

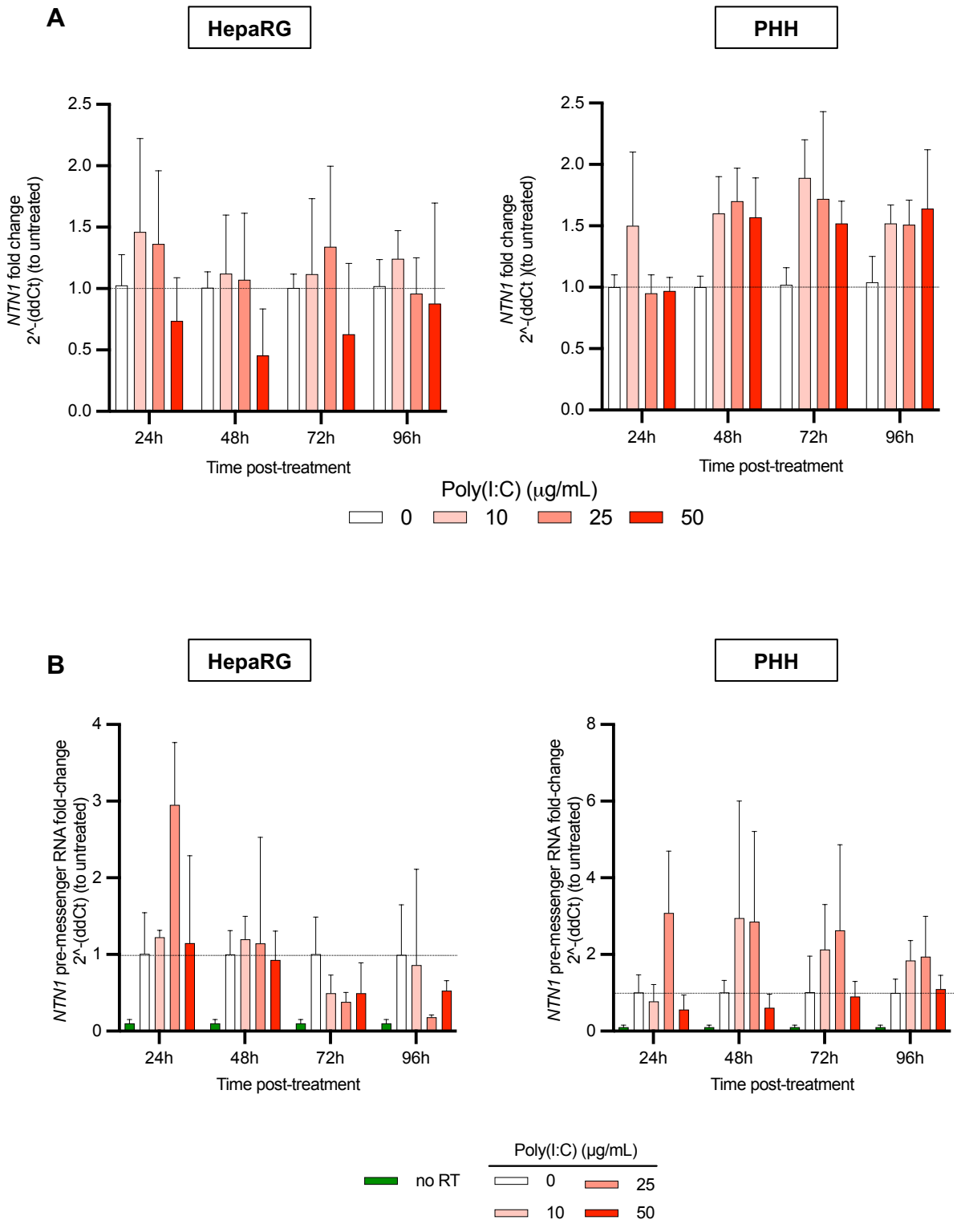

Supplementary figure 8

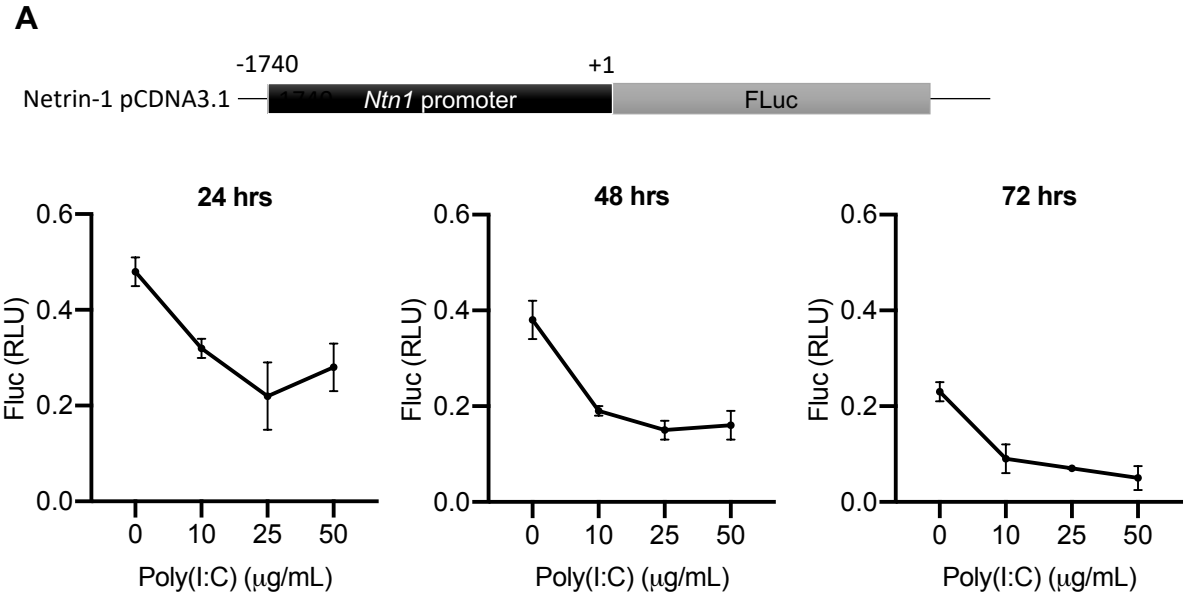

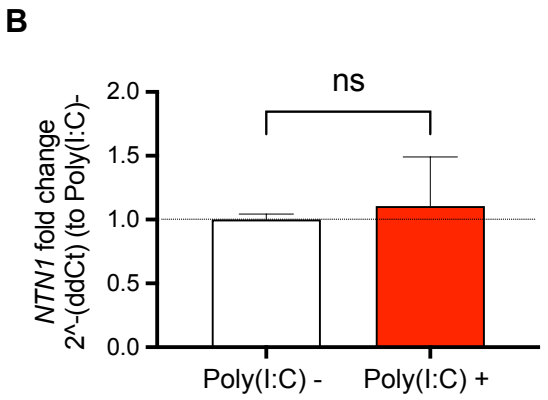

Supplementary figure 9

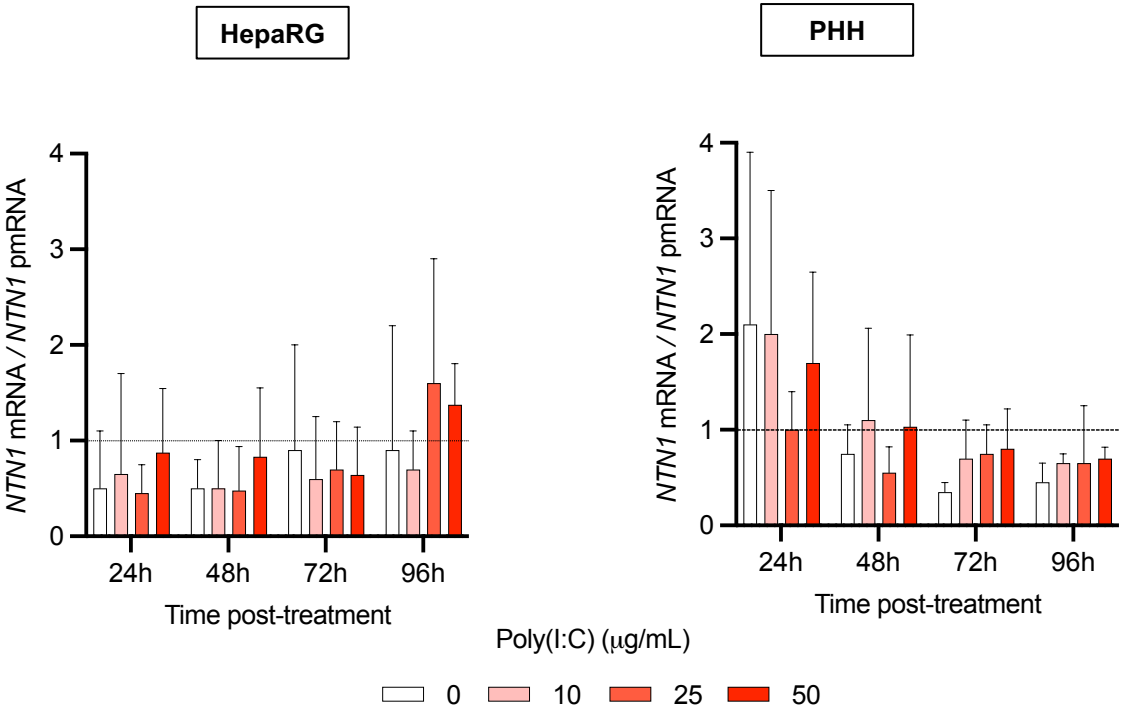

Supplementary figure 10

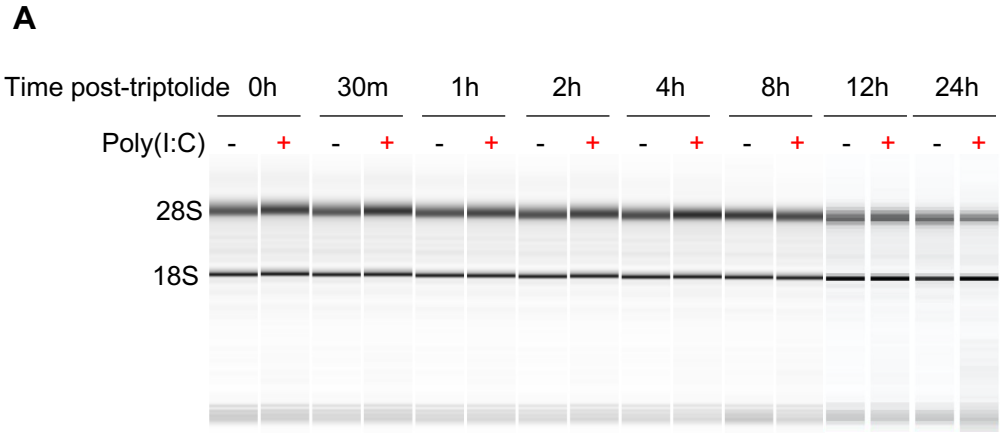

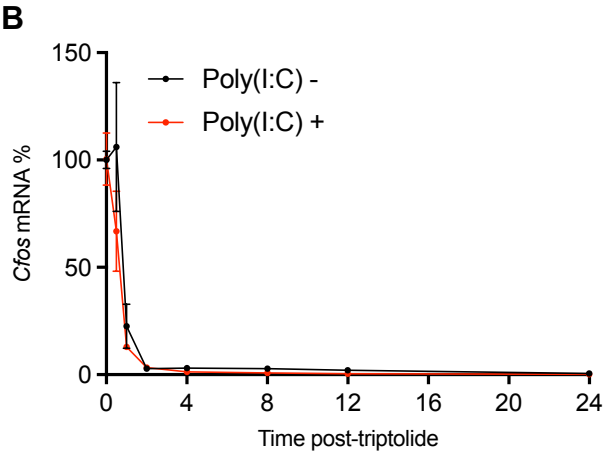

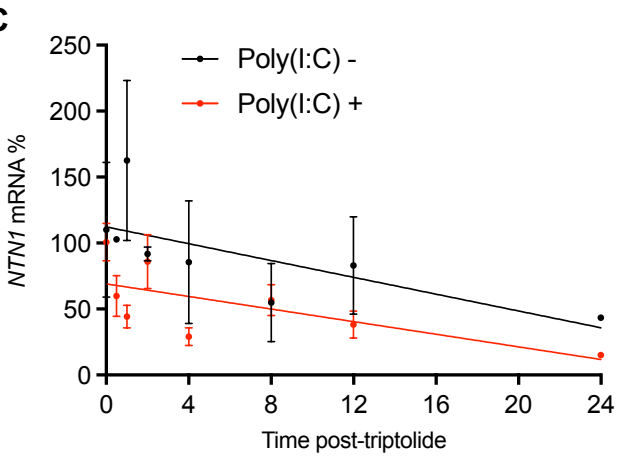

	Poly(I:C)-	Poly(I:C)+
Slope	-3.186 ± 1.255	-2.388 ± 1.030

Supplementary figure 11

A

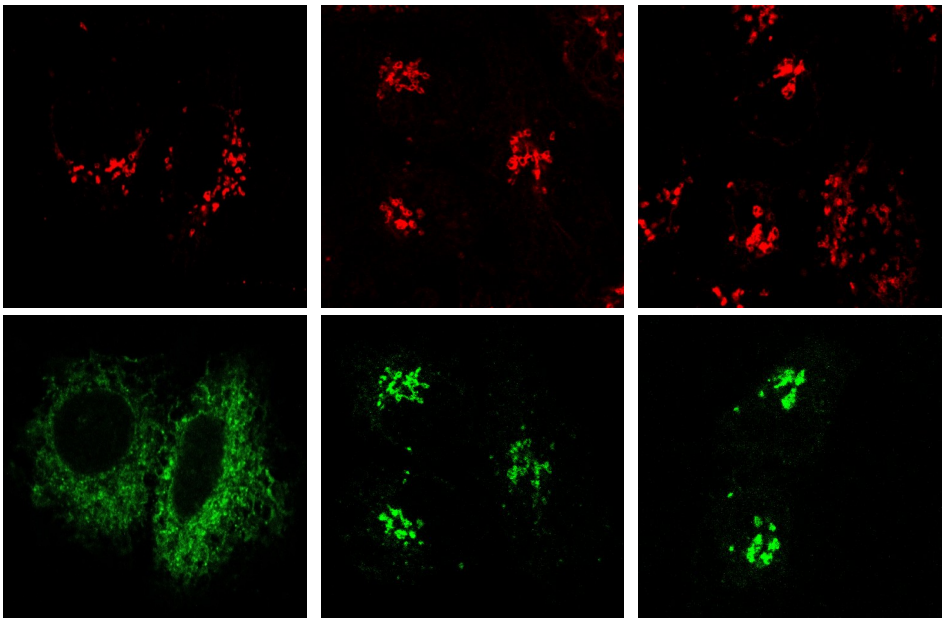

B

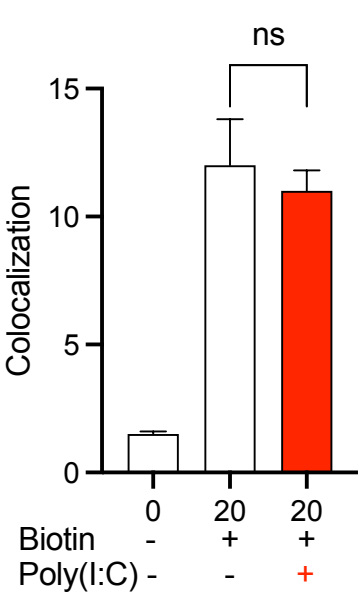

Supplementary figure 12

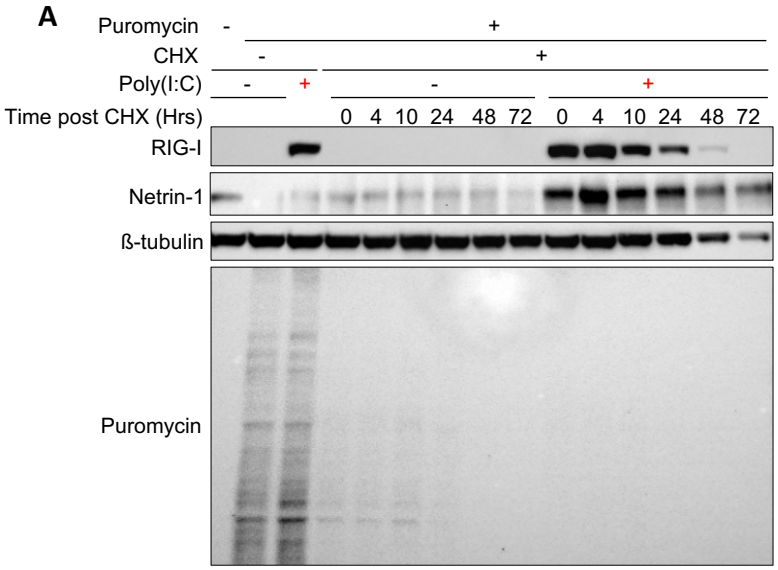

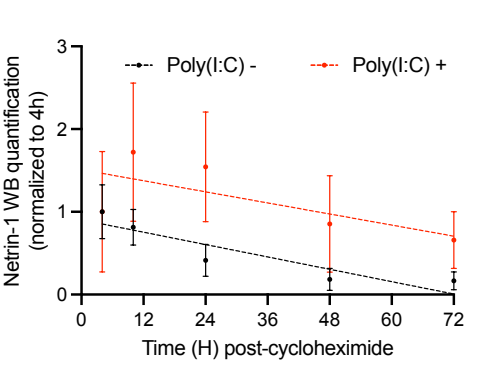

	Poly(I:C)-	Poly(I:C)+
Slope	-0.01245 ± 0.001875	-0.01116 ± 0.005271

Supplementary figure 13

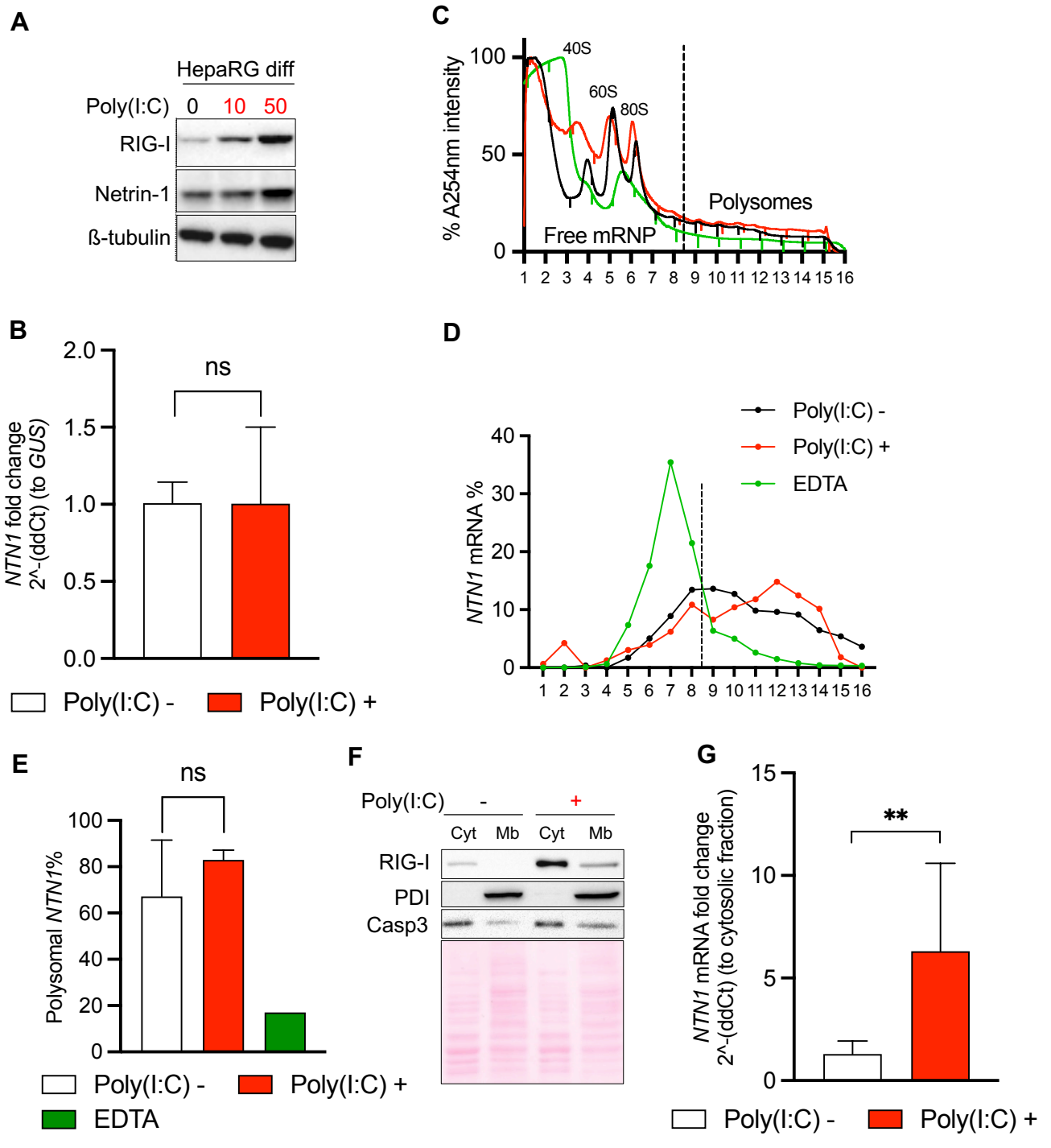

Supplementary figure 14

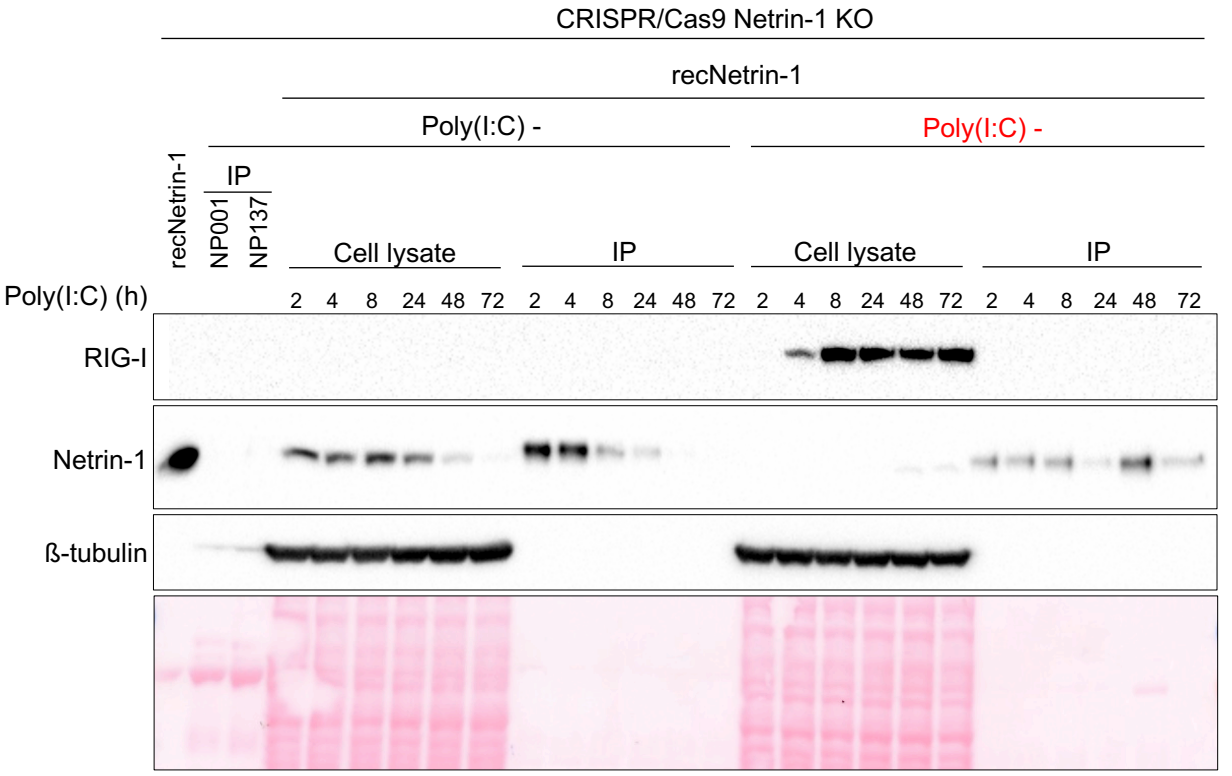

Supplementary figure 15